NASA/CR—2005-213870

Phased-Array Study of Jets With Various Internal Mixers and Nozzles

Sang Soo Lee
QSS Group, Inc., Cleveland, Ohio

September 2005

The NASA STI Program Office . . . in Profile

Since its founding, NASA has been dedicated to the advancement of aeronautics and space science. The NASA Scientific and Technical Information (STI) Program Office plays a key part in helping NASA maintain this important role.

The NASA STI Program Office is operated by Langley Research Center, the Lead Center for NASA's scientific and technical information. The NASA STI Program Office provides access to the NASA STI Database, the largest collection of aeronautical and space science STI in the world. The Program Office is also NASA's institutional mechanism for disseminating the results of its research and development activities. These results are published by NASA in the NASA STI Report Series, which includes the following report types:

- TECHNICAL PUBLICATION. Reports of completed research or a major significant phase of research that present the results of NASA programs and include extensive data or theoretical analysis. Includes compilations of significant scientific and technical data and information deemed to be of continuing reference value. NASA's counterpart of peer-reviewed formal professional papers but has less stringent limitations on manuscript length and extent of graphic presentations.

- TECHNICAL MEMORANDUM. Scientific and technical findings that are preliminary or of specialized interest, e.g., quick release reports, working papers, and bibliographies that contain minimal annotation. Does not contain extensive analysis.

- CONTRACTOR REPORT. Scientific and technical findings by NASA-sponsored contractors and grantees.

- CONFERENCE PUBLICATION. Collected papers from scientific and technical conferences, symposia, seminars, or other meetings sponsored or cosponsored by NASA.

- SPECIAL PUBLICATION. Scientific, technical, or historical information from NASA programs, projects, and missions, often concerned with subjects having substantial public interest.

- TECHNICAL TRANSLATION. English-language translations of foreign scientific and technical material pertinent to NASA's mission.

Specialized services that complement the STI Program Office's diverse offerings include creating custom thesauri, building customized databases, organizing and publishing research results . . . even providing videos.

For more information about the NASA STI Program Office, see the following:

- Access the NASA STI Program Home Page at ***http://www.sti.nasa.gov***

- E-mail your question via the Internet to help@sti.nasa.gov

- Fax your question to the NASA Access Help Desk at 301–621–0134

- Telephone the NASA Access Help Desk at 301–621–0390

- Write to:
  NASA Access Help Desk
  NASA Center for AeroSpace Information
  7121 Standard Drive
  Hanover, MD 21076

NASA/CR—2005-213870

Phased-Array Study of Jets With Various Internal Mixers and Nozzles

Sang Soo Lee
QSS Group, Inc., Cleveland, Ohio

Prepared under Contract SAA3–456

National Aeronautics and
Space Administration

Glenn Research Center

September 2005

Available from

NASA Center for Aerospace Information
7121 Standard Drive
Hanover, MD 21076

National Technical Information Service
5285 Port Royal Road
Springfield, VA 22100

Available electronically at http://gltrs.grc.nasa.gov

Phased-Array Study of Jets With Various Internal Mixers and Nozzles

Sang Soo Lee
QSS Group, Inc.
Cleveland, Ohio 44135

The 16 microphone linear phased-array system has been successfully applied to identify the noise source locations. The various mixers and nozzles increase or decrease noise levels of certain frequency components. The phased-array beamforming can show the locations of these added/decreased noise sources. It was also able to detect any internal rig noise that is shown to be coming from the nozzle exit. Major beamforming level differences between nozzles occurs at the nozzle exit. Among the three nozzles tested, the medium length nozzle was the quietest for all mixers. The spectrum levels of the high penetration 12-lobed mixer are much higher than the low penetration mixer in the frequency ranges higher than 1 or 1.5 kHz. The high penetration 20-lobed 20UH mixer has lower spectrum levels than the 12-lobed mixer in the high frequency range above about 1 or 1.5 kHz. Introducing a deep scallop was successful in reducing mixer noise in most frequencies.

1. Introduction

This report presents the results of the phased-array test cosponsored by the NASA Quiet Aircraft Technology program and Allison Advanced Development Corporation. This test was conducted in the Nozzle Acoustic Test Rig (NATR) in the NASA Glenn Research Center by using the model hardware first tested in 1996 (Mengle, Baker and Dalton, 2002). This model rig represented a turbofan engine exhaust configuration employing forced mixing between the secondary fan and primary core flow streams. Three nozzles and six mixer configurations including those produced the lowest and highest levels of the measured noise from the previous test are tested. These configurations were tested on subsonic operating conditions.

The far field noise data obtained during previous 1996 tests showed a wide variation in the far field noise levels for a fixed thrust level. While certain general trends could be identified from this data, it was not possible to explain these trends in detail. Therefore, in this test, additional diagnostic measurements were used for an improved understanding of the noise generation process when forced mixing is present. The results from the phased-array analyses are presented in this paper. Meanwhile, results from the PIV tests were presented in Bridges and Wernet (2004) and the analysis of the far-field acoustics were given by Tester and Fisher (2004).

The linear phased-array was composed of 16 microphones positioned at unequal intervals in one-dimensional direction. Two different settings of the phased-array system, one mounted on the floor and the other mounted in the overhead position, are used in this test. Both arrays were installed in parallel with the jet-flow centerline. The classical beamforming method is used in the beamforming image processing.

In section 2, summary of the test hardware, test conditions, microphone positions, data processing and phased-array beamforming method will be presented. The array pattern, point source response, internal rig noise, repeatability of test points, and effect of venturi nozzle are given in section 3. The effect of nozzles will be discussed in section 4 and that of mixers will be given in section 5.

2. Experimental Setup and Phased-Array Beamforming Method

2.1 Test Hardware and Test Conditions

The test was conducted in the NASA Glenn Research Center AeroAcoustic Propulsion Laboratory (AAPL). The AAPL is a 65 ft radius anechoic hemispherical dome. Its walls and approximately half of the floor area are covered by acoustic wedges. The Nozzle Aeroacoustic Test Rig (NATR) in the AAPL provides the airflow for the flight simulation capability. The NATR duct is acoustically lined and consists of an annular ejector system connected to a plenum followed by the transition section which is an ASME long-radius, low beta venturi nozzle. This flow is exhausted through a second nozzle of 53 in. diameter which forms a free jet to simulate the effects of forward flight on the test article. The centerline of the free jet is 10 ft above the floor. The maximum Mach number of the free jet is 0.3. An acoustically treated wall separates the NATR from the section of the building which does not have acoustic treatment on the floor.

Downstream of the NATR is the Dual Flow Jet Exit Rig (DFJER2). The DFJER2 is the structure through which airflow is delivered from the facility compressed air system to the test article. This hardware has been recently redesigned and refitted in order to reduce the levels of internal flow noise. The test article is attached to the aft end of the DFJER2.

The mixed flow exhaust system model hardware consists of co-annular fan and core flow ducts, forced mixer and exhaust nozzle. Three different nozzles, L0, L1, and L2 were tested. The nozzle lengths from the mixer plane are 1.53, 1.16, and 0.78 nozzle diameters, respectively, as shown in Figure 2.1. All nozzles have a nominal cold throat diameter of 7.245 in. and a nominal cold throat area of 41.225 in.^{2}. Data obtained from both current and previous tests show a substantial reduction in far field noise levels when the length of the L1 nozzle was shortened by 25 percent from the baseline L0 nozzle. However, further reduction in nozzle mixing length did not result in lower noise level as the shortest one L2 was noisier than the medium length L1. The phased-array analyses will be used to show the details of the nozzle effect.

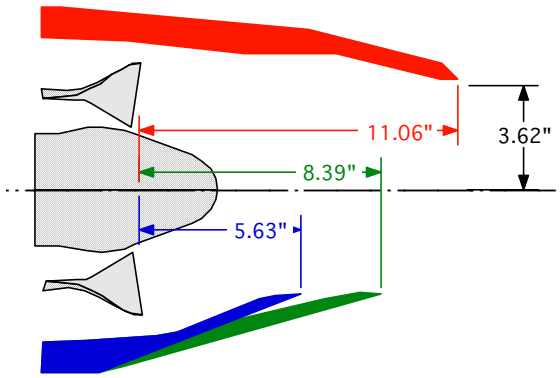

Figure 2.1.—Lengths and internal contours of nozzles L0(red), L1(green), and L2(blue).

Figure 2.2 shows the pictures of the confluent axisymmetric splitter and five configurations of lobed mixer tested in this study. These configurations represent a substantial variation of the important geometric parameters of a lobed mixer. The confluent axisymmetric splitter, Con is served as the baseline configuration. Three 12-lobed mixers are tested in order to understand the effect of mixer penetration. The low, intermediate and high penetration mixers, 12CL, 12UM, and 12UH have peak to peak penetrations of 0.5, 0.7, and 0.88 of the mixer plane annulus, respectively. Two 20-lobed mixers, 20UH and 20DS are used to study the effect of lobe width and scallop. Both 20-lobed mixers have the same high penetration as the 12UH mixer. The 20DS mixer has deep scallops.

Figure 2.2.—Pictures of mixers: 12CL (top left), 12UM (top center), 12UH (top right), Con (bottom left), 20UH (bottom center) and 20DS (bottom right).

Results from three flow conditions are presented in this paper. The core and fan (bypass) flow conditions of the set points 110 and 310 are listed in Table 2.1. The set point 5000 where both core and fan streams have the same pressure ratio without heating was used to mimic the single flow cold jet. There is no free jet in all three set points. Overall rig operational parameters are monitored and recorded through the ESCORT data system. Each data point is identified by the ESCORT number.

More detailed information on the test hardware and flow conditions can be found in Bridges and Wernet (2004) where the results of the Particle Image Velocimetry (PIV) are presented.

TABLE 2.1.—DEFINITION OF SET POINTS AND FLOW CONDITIONS.

Set point id	Core NPR	Fan NPR	Core NTR	Fan NTR	Free jet Mach No
110	1.39	1.44	2.799	1.196	0
310	1.74	1.82	3.337	1.196	0
5000	1.435	1.435	1	1	0

2.2 16 Microphone Linear Phased Array

The phased array was composed of 16 microphones positioned at unequal intervals. We have tried two different settings of the phased-array system, one mounted on the floor and the other mounted in the overhead position as shown in Figure 2.3. Both arrays are installed in parallel with the jet-flow centerline. The microphones in the floor array were flush mounted without the protective grids. However, those in the overhead array are mounted on microphone holders and the protective grids were used. It will be shown in section 3.4 that the overhead array is possibly exposed to the external hardware noise from the pipes as well as from the core and bypass venturi nozzles located upstream of the jet exit. Meanwhile, the external noise from the pipes below the nozzle might affect the floor array.

Microphone positions in both array systems are shown in Figure 2.4. The origin of the right-handed Cartesian coordinate system is located at the center of the L0 nozzle exit plane. The x coordinate is on the jet centerline with positive values in the jet-flow downstream direction. The x and y coordinates are

parallel with and the z coordinate is perpendicular to the floor. The microphone number 1 of the floor array is located in the upstream location, but the numbering of microphones was reversed for the overhead array. The coordinates of microphones are given in appendix A. The distances from each microphone to the center of the L0, L1 and L2 nozzle exit planes are given with the microphone angles (in degrees) from the negative x axis. The distances and the angles are also shown for the mixer only case where the nozzle was not installed.

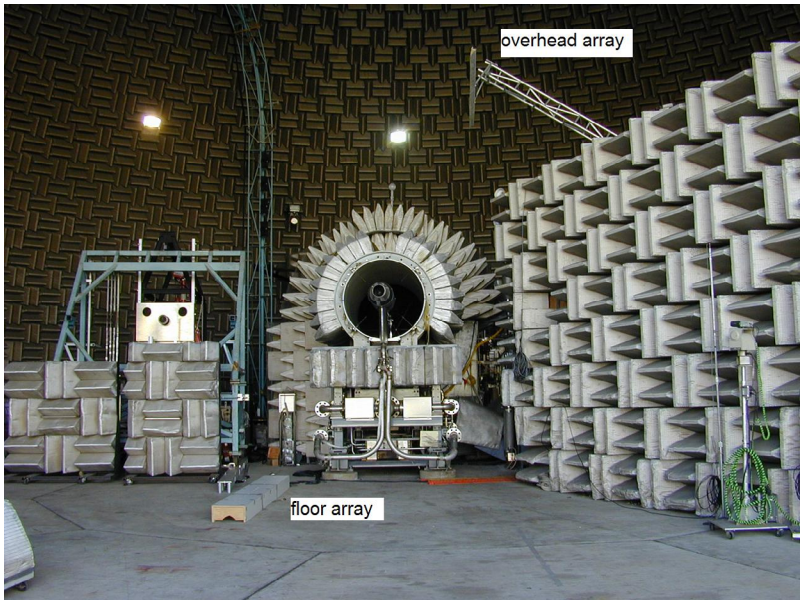

Figure 2.3.—Floor and overhead phased-array systems.

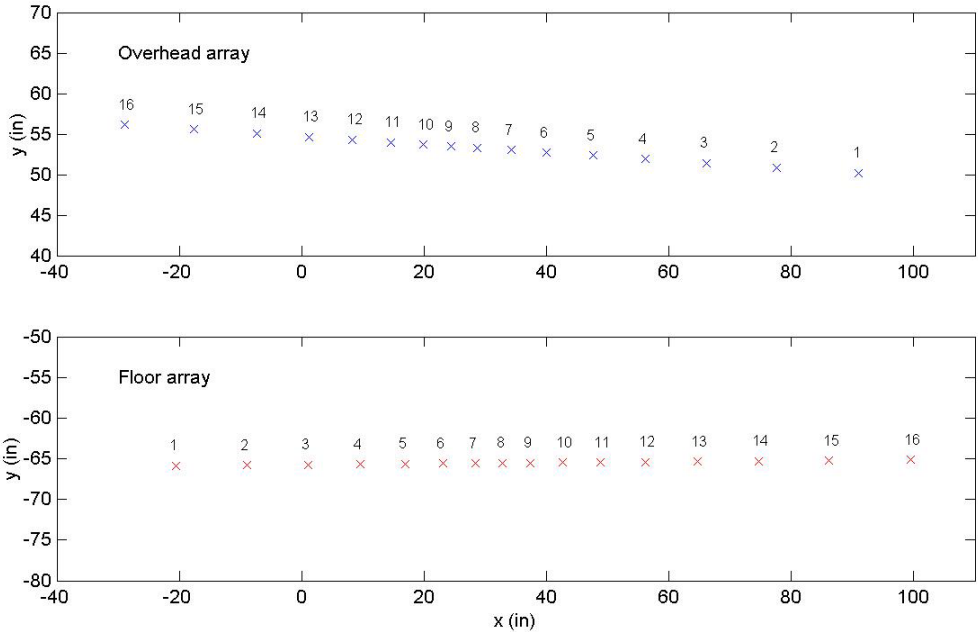

Figure 2.4.—Microphone positions in floor and overhead arrays.

2.3 Data Processing

The far-field 1/4 in. condenser microphones are used to measure sound pressure level. The microphone preamplifiers are connected to the four-channel microphone conditioning amplifiers, B&K Nexus 2690 units. The outputs of the Nexus 2690 are connected into the Datamax data acquisition system. The sampling rate of the Datamax system was 200 kHz with the bandwidth of 90 kHz. All 16 microphone signals are recorded simultaneously for 40 seconds. The calibration constants of microphones are obtained by using a 250 Hz single frequency piston phone. The 'as measure' signals are used to compute narrowband spectra and beamforming outputs presented in this paper. For the cross-spectral density calculations, the Matlab function 'csd' was used with 8192 data points, 50 percent overlapping and Hanning's periodic window. All beamforming analyses have been performed based on the narrowband cross-spectral densities with bandwidth of 24.41 Hz.

2.4 Classical Beamforming Method

The phased-array analysis was conducted by using a code developed at NASA Glenn Research Center. The classical beamforming method that is summarized in this section will be used to analyze the data.

If there are M monopole point sources $s_m(t)$ located at $\vec{X}_{sm}$, for $m = 1,2,\ldots, M$, the near-field sound pressure measured by the nth microphone becomes

$$p_n(t) = \sum_{m=1}^{M} \frac{1}{r_{nm}} s_m\left(t - \frac{r_{nm}}{c}\right),$$

where

$$r_{nm} = \left|\vec{x}_n - \vec{X}_{sm}\right|$$

is the distance between the nth microphone and the mth point source. The microphones of the phased array are located at $\vec{x}_n$ for $n = 1,2,\ldots, N,$. The Fourier transform $P_n(\omega)$of $p_n(t)$ becomes

$$P_n(\omega) = \int_{-\infty}^{\infty} p_n(t) e^{-j\omega t} dt = \sum_{m=1}^{M} \frac{1}{r_{nm}} \exp(-j\omega r_{nm}/c) S_m(\omega),$$

where $S_m(\omega)$ is the Fourier transform of $s_m(t)$

$$S_m(\omega) = \int_{-\infty}^{\infty} s_m(t) e^{-j\omega t} dt.$$

Since the length of the measured microphone signal is finite, $p_n(t)$ is equal to zero everywhere except the finite segment $0 \le t \le T$. The two-sided cross-spectral density per unit time, $\hat{P}_{i,k}(f)$, is defined as the Fourier transform of the correlation of $p_i(t)$ and $p_k(t)$ divided by T,

$$\hat{P}_{i,k}(f) = \frac{P_i(f) P_k^*(f)}{T} = \sum_{m=1}^{M} \sum_{n=1}^{M} C_{im} \hat{S}_{m,n}(f) C_{kn}^*, \quad -\infty < f < \infty$$

where

$$C_{im} = \frac{\exp(-j2\pi f r_{im} / c)}{r_{im}}$$

$$\hat{S}_{m,n}(f) = \frac{S_m(f) S_n^{*}(f)}{T} = \frac{1}{T}\int_{-\infty}^{\infty} e^{-j2\pi ft} Corr(s_m, s_n) dt$$

and $\hat{S}_{m,n}(f)$ is the two-sided cross-spectral density per unit time of the sources $s_m(t)$ and $s_n(t)$. When the functions $p_i(t)$, $p_k(t)$, $s_m(t)$ and $s_n(t)$ are real, we can show that $\hat{P}_{i,k}(-f) = \hat{P}_{i,k}^{*}(f)$ and $\hat{S}_{m,n}(-f) = \hat{S}_{m,n}^{*}(f)$.

It is convenient to write the above equation in a matrix form

$$\hat{\mathbf{P}} = \mathbf{C}\hat{\mathbf{S}}\mathbf{C}^{+}$$

where $\hat{\mathbf{P}}$ is a N by N matrix, $\mathbf{C}$ is a N by M matrix, $\hat{\mathbf{S}}$ is a M by M matrix and $\mathbf{C}^{+}$ is the Hermitian conjugate of $\mathbf{C}$, i.e., the complex conjugate of the transpose of $\mathbf{C}$. If the sources are mutually uncorrelated, then the matrix $\hat{\mathbf{S}}$ is diagonal.

In order to focus the phased array at an arbitrary position, $\vec{X}$, the steering vector $\mathbf{H}$, that is $[H_1, H_2, ..., H_N]$, is obtained as

$$H_n = \tilde{\alpha} \exp\left(\frac{j2\pi f \tilde{r}_n}{c}\right)$$

where $\tilde{r}_n = \left|\vec{x}_n - \vec{X}\right|$ and $\tilde{\alpha}$ is the normalization constant defined as

$$\tilde{\alpha} = \frac{1}{\sum_{n=1}^{N} 1/\tilde{r}_n}$$

By multiplying $\mathbf{H}$, we can obtain

$$\mathbf{H}\hat{\mathbf{P}}\mathbf{H}^{+} = \mathbf{K}\hat{\mathbf{S}}\mathbf{K}^{+}$$

where

$$\mathbf{K} = \mathbf{H}\mathbf{C} = \left[K_1, K_2, ..., K_M\right]$$

with

$$K_m = \tilde{\alpha} \sum_{n=1}^{N} \frac{1}{r_{nm}} \exp\left[\frac{-j2\pi f (r_{nm} - \tilde{r}_n)}{c} \right]$$

If the focal point $\vec{X}$ coincides with the mth source location $\vec{X}_{sm}$, then K_m becomes equal to 1.

If there is only one monopole source, i.e. $M = 1$, then

$$\hat{\mathbf{S}} = \hat{S}_{1,1}(f) = \frac{1}{T} |S_1(f)|^2$$

$$\mathbf{K} = K_1 = \tilde{\alpha} \sum_{n=1}^{N} \frac{1}{r_{n1}} \exp\left[\frac{-j2\pi f (r_{n1} - \tilde{r}_n)}{c} \right]$$

We can also show that

$$|\mathbf{K}|^2 = \frac{\tilde{\alpha}^2}{r_s^2} |W|^2 ,$$

where r_s is the distance between the source and the origin of the coordinate system and W is the array pattern defined in the previous section. When the focal point $\vec{X}$ coincides with the monopole source location $\vec{X}_{s1}$, then **K** becomes equal to 1 independently of the frequency f and

$$\mathbf{H}\hat{\mathbf{P}}\mathbf{H}^{+} = \hat{S}_{1,1}(f) .$$

If sound sources are mutually uncorrelated, then

$$\hat{S}_{m,n} = 0 \quad \text{for} \quad m \neq n ,$$

and

$$\mathbf{H}\hat{\mathbf{P}}\mathbf{H}^{+} = \sum_{m=1}^{M} |K_m|^2 \, \hat{S}_{m,m}(f) .$$

3. Array Property and Internal Rig Noise

3.1 Array Pattern and Point Sound Source Response

The array pattern of the floor array with a source at x/D = 0, where D represents the nozzle diameter of 7.245 in., is given in Figure 3.1. The contour plot of the array patterns computed at narrowband frequencies is plotted on left side with the color bar of 20 dB scale. The peak locations and –1 and –3 dB contour lines are plotted on right side. The peak locations and –1 dB contour lines for the floor and overhead array when a single source is located at x/D = 0, 5 or 10 are given in Figure 3.2.

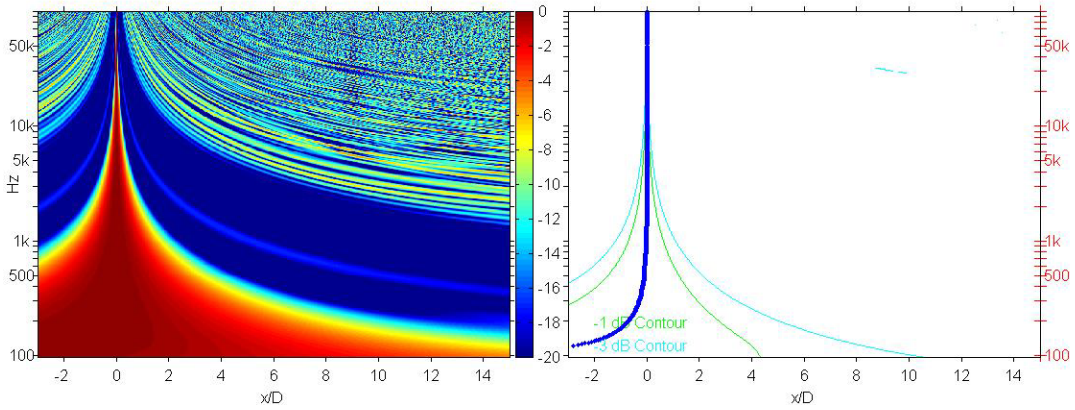

Figure 3.1.—Array pattern of the floor array with a source at x/D = 0.

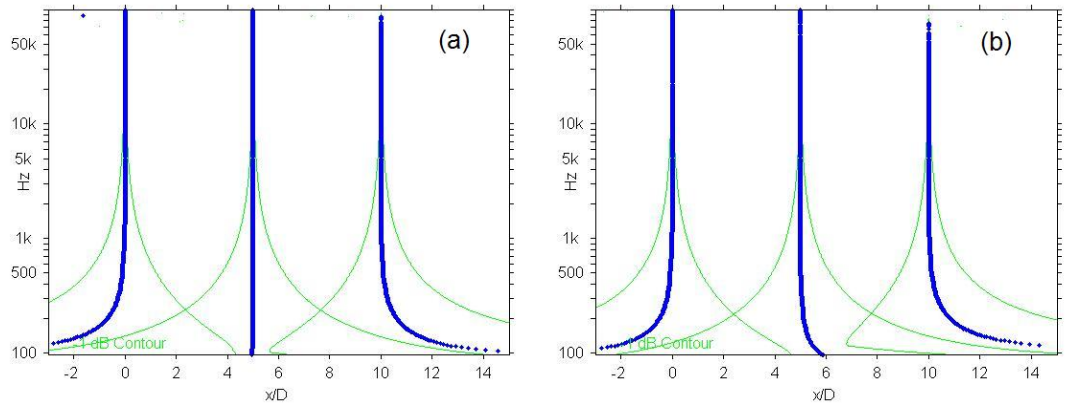

Figure 3.2.—Peak locations and -1 dB contour lines of the array patterns with a single source at x/D = 0, 5 or 10 for (a) floor array and (b) overhead array.

Figures 3.1 and 3.2 show that the –1 and –3 dB beam widths of both arrays are small for the most frequencies of our interest. For low frequencies, below 300 or 400 Hz, the peak locations do not agree with the source locations and –1 dB beam widths become large. The difference between the floor and overhead arrays in Figure 3.2 is mainly due to different streamwise microphone locations as shown in Figure 2.4.

The beamforming results from the floor array with an impinging jet located at about 1.2 nozzle diameters from the L0 nozzle exit are given in Figure 3.3. Compressed air coming out from a 1/4 in. nozzle is impinging on a small perpendicular plate to mimic a point sound source. The classical beamforming method is used to calculate the beamforming levels along the jet centerline for all narrowband frequencies. At each frequency the peak location and peak level, given in the first two columns in the second row, are found from the streamwise location where the maximum beamforming level occurs. The contour plots of beamforming levels are given in the first row in Figure 3.3. The beamforming levels normalized by the peak level at each frequency are used in the upper-left contour plot with 20 dB color bar scale. Meanwhile, the contour plot of the absolute beamforming levels is shown in the upper-right figure with the color bar in dB scale. The narrowband spectra for all 16 microphones are plotted in the bottom-right figures. Those of the back ground noise (escort number, 1774) are plotted with dotted curves.

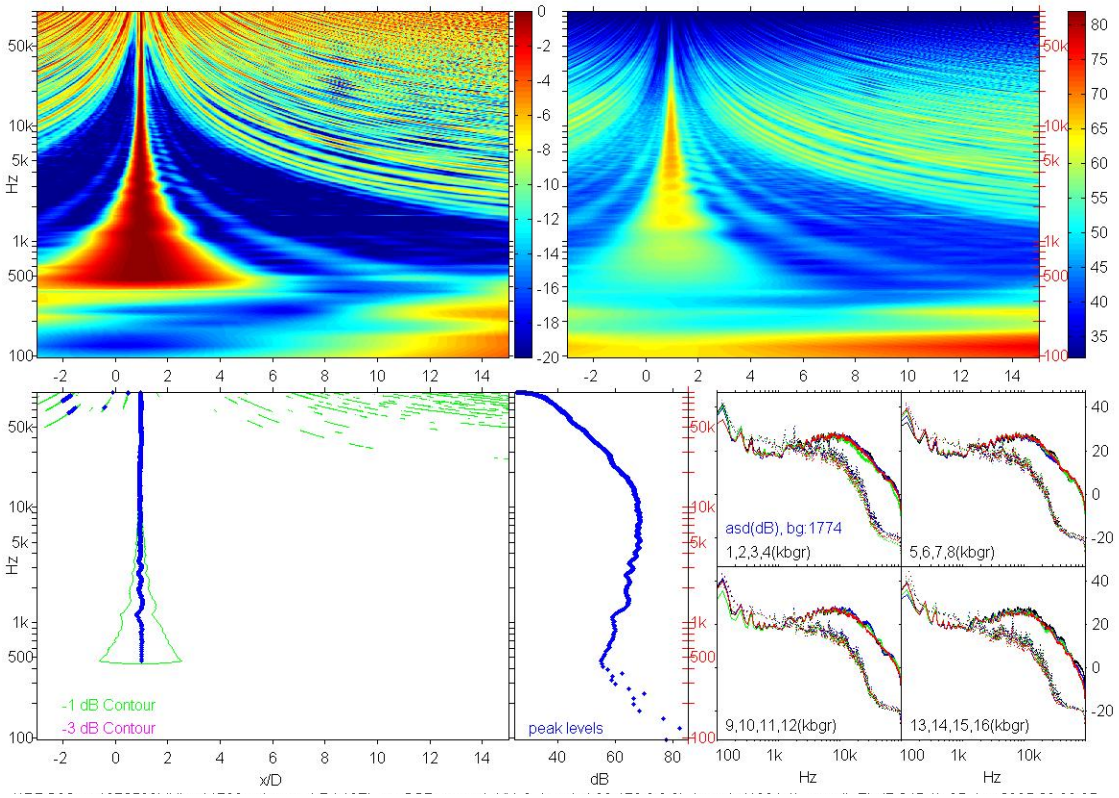

Figure 3.3.—Classical beamforming results of impinging jet noise source with floor array (escort number: 1768).

This floor array is shown to be very successful to find noise source locations for the frequencies higher than 450 Hz. Since the microphone positions are accurately known, the beamforming analysis can produce accurate peak locations up to the Nyquist critical frequency, 100 kHz. The noise level produced by the impinging jet is as low as the back ground level for the frequencies below 1 kHz as shown in the narrowband spectra.

Figure 3.4 shows the contour plots of normalized and absolute beamforming levels, peak locations and peak levels when an acoustic sound source is used for the same floor array. One end of a 10-ft-long steel pipe of 1 in. diameter is connected to an acoustic driver and the other open end is positioned at about 1.3D from the nozzle exit on the jet centerline. The acoustic driver is driven by an amplifier and white noise generator. It is shown that the peak locations between 400 Hz and 50 kHz are accurately found.

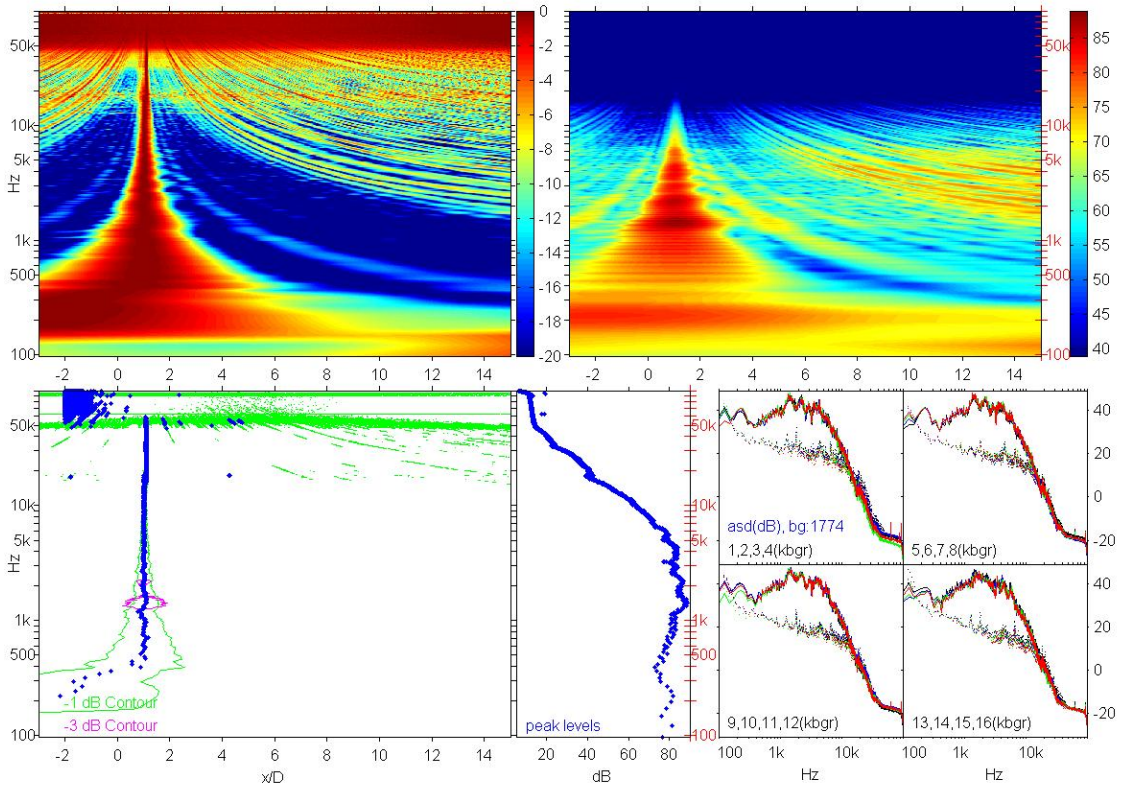

Figure 3.4.—Classical beamforming results of white noise acoustic sound source with floor array (escort number: 1772).

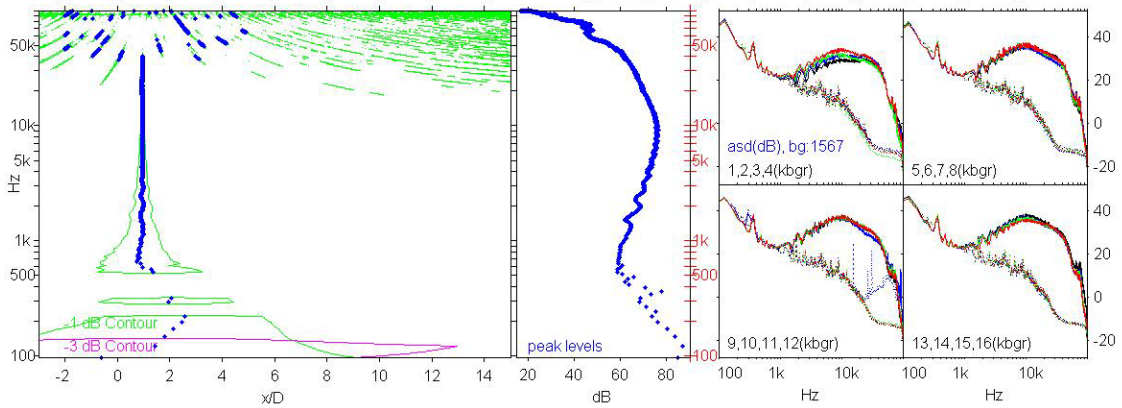

Figure 3.5.—Classical beamforming results of impinging jet noise source with overhead array (escort number: 1568).

The classical beamforming results of the overhead array for the impinging jet and acoustic sound source are given in Figure 3.5 and 3.6, respectively. Figure 3.5 shows that the location of the impinging jet is successfully found in the frequency range between 600 Hz and 40 kHz. The poor response in the high frequency range above 40 kHz is due to the uncertainty in measuring microphone positions of the overhead array. In Figure 3.6, peak locations agree with the acoustic sound source location in the 300 Hz and 40 kHz range.

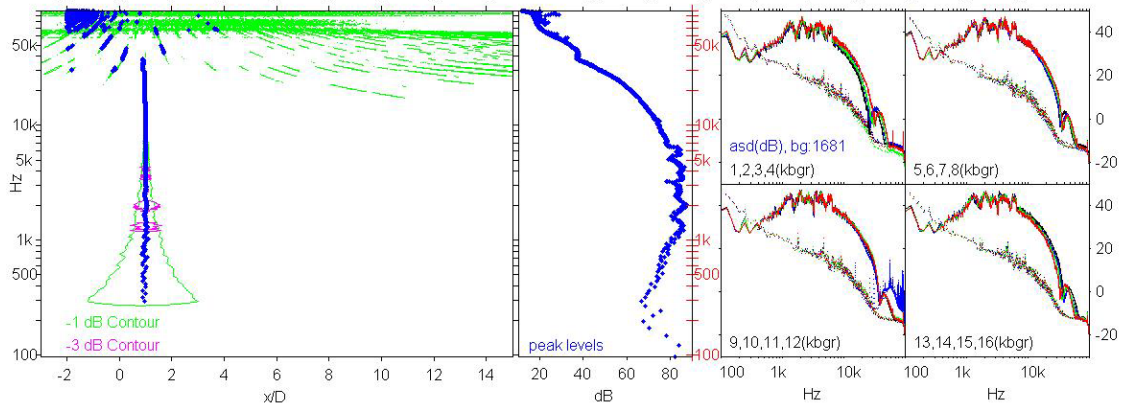

Figure 3.6.—Classical beamforming results of white noise acoustic sound source with overhead array (escort number: 1678).

3.2 Internal Core Rig Noise

The confluent splitter was tested without a nozzle in order to understand the strength of the internally generated core rig noise. Different core pressure ratios, 1.05, 1.07, 1.10, 1.14, 1.17, 1.22, 1.28, 1.34, and 1.42 are used while the core temperature ratios are kept constant between 3.18 and 3.20. Although there is no nozzle, we had very low fan flow pressure ratio, about 1.02, in order to cool the hardware. The floor array was used without the free jet.

Figure 3.7 shows the auto-spectral densities, as measured, from the microphones 2, 4, 9, and 16. The microphone angles measured from the negative x-axis relative to the center of the confluent splitter exit plane are 90.9, 99.1, 110.5, and 130.6°, respectively. Figures 3.8, 3.9, and 3.10 show the peak levels, peak locations and contour plots of the normalized beamforming levels from the classical beamforming method.

Figures 3.9 and 3.10 show that there are two locations where the internally generated rig noises are coming out, one at the confluent splitter exit and the other at the opening for the fan flow (located at about 0.33D upstream of the mixer exit). Contrast to the internal noise whose peak location appears at the mixer or nozzle exit, the peak locations of the jet noise are dependent on the frequency. As shown in Figure 3.9, the jet noise peak location gradually moves from downstream positions to the splitter exit as frequency changes from low to high. It is shown in Figures 3.1 and 3.2 that the floor array is not able to predict the accurate peak locations at low frequencies below 300 or 400 Hz.

In the low nprc case, for example when nprc is 1.10, the internal noise from the fan flow opening dominates the high frequency range above 15 kHz, the core internal noise dominates mid frequencies between 2 and 15 kHz, and the jet noise is the strongest in the low frequencies below 2 kHz. As jet velocity becomes higher, the jet flow noise becomes stronger relative to the increase of the internal rig noise. When nprc is 1.42, the jet noise becomes dominant for the frequencies up to 30 kHz. The noise from the splitter exit, however, is still stronger than the jet noise at higher frequencies even at this highest velocity point.

It is shown in Figure 3.10 that there is a strong 2 kHz noise at x/D is about 1.5 for all jet velocities considered. High frequency tones, at about 10 to 40 kHz, are also shown in the spectral densities, especially at microphone number 9 in Figure 3.7.

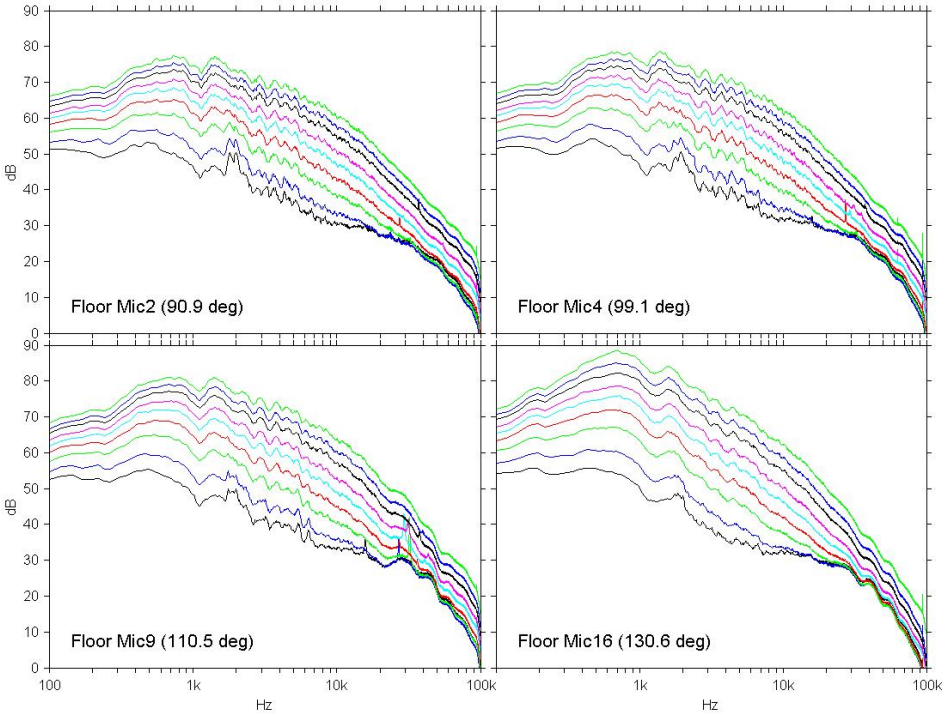

Figure 3.7.—Narrowband spectra for confluent splitter without nozzle: nprc = 1.05, 1.07 1.10, 1.14, 1.17, 1.22, 1.28, 1.34, and 1.42 from bottom to top (escort numbers: 1845 to 1853, respectively).

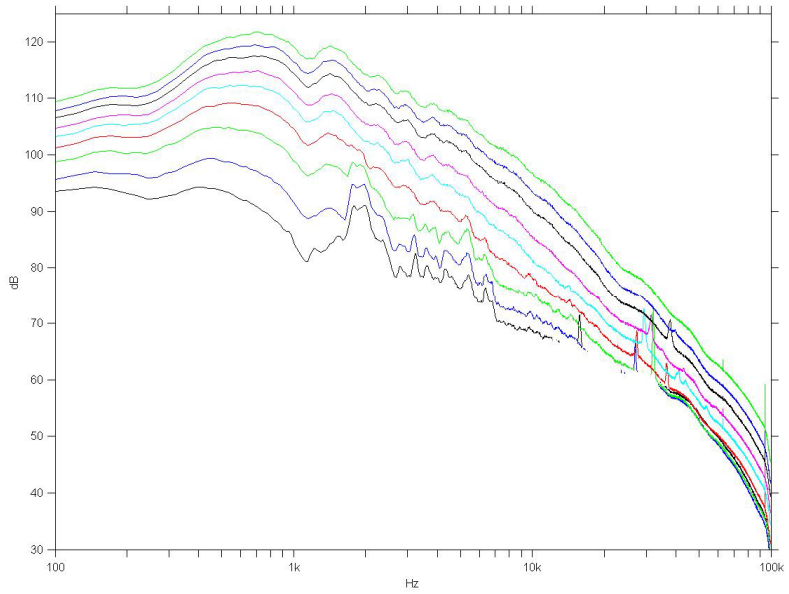

Figure 3.8.—Peak levels from classical beamforming method for confluent splitter without nozzle: nprc = 1.05, 1.07 1.10, 1.14, 1.17, 1.22, 1.28, 1.34, and 1.42 from bottom to top.

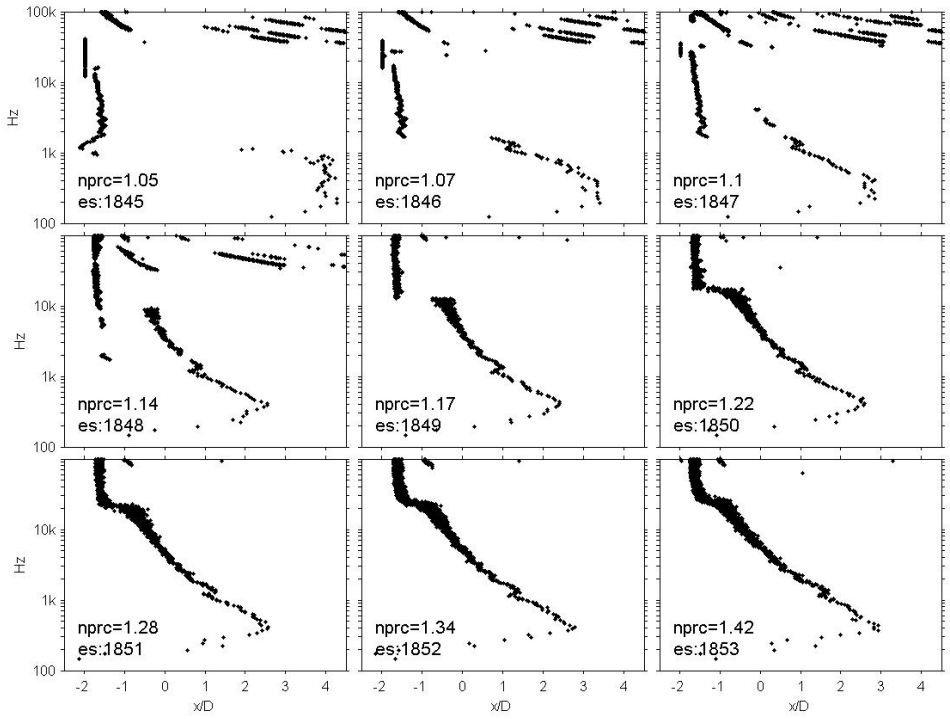

Figure 3.9.—Peak locations for confluent splitter without nozzle: nprc = 1.05, 1.07 1.10, 1.14, 1.17, 1.22, 1.28, 1.34, and 1.42.

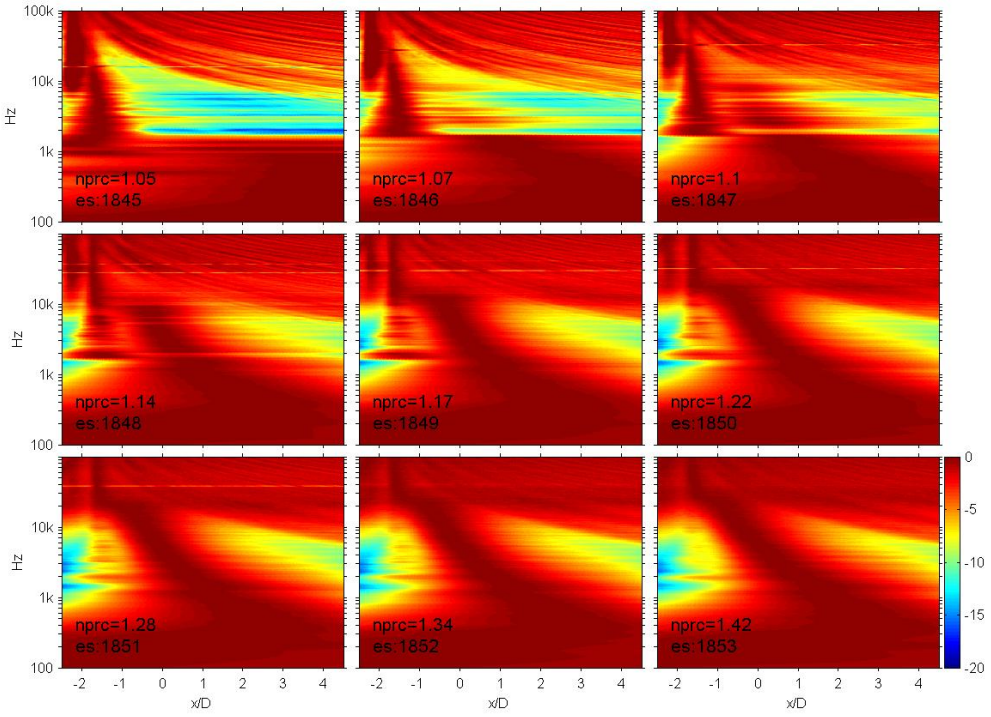

Figure 3.10.—Contour plots of normalized beamforming levels for confluent splitter without nozzle: nprc = 1.05, 1.07 1.10, 1.14, 1.17, 1.22, 1.28, 1.34, and 1.42.

3.3 Repeatability

In order to verify the repeatability in flow conditions and the sensitivity of the beamforming results, the same set point has been hit twice for the same hardware. Figure 3.11 shows the results for the 12CL mixer with L1 nozzle at the set point 310. The x coordinate is shifted so that the origin is now at the L1 nozzle exit. The narrowband spectra from the overhead microphone at 112° show essentially identical response from both data. The beamforming level differences between two readings are within –0.7 and 0.9 dB.

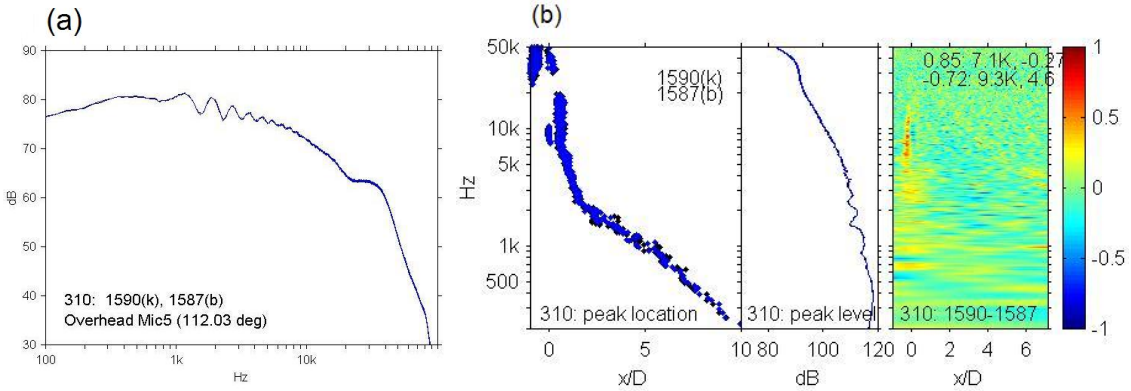

Figure 3.11.—(a) Narrowband spectra and (b) beamforming results for 12CL mixer with L1 nozzle at set point 310 (escort numbers: 1590 and 1587).

Similar results are obtained at the set point 310 for the 12CL mixer with the L0 nozzle (escort numbers: 1581 and1584) and L2 nozzles (escort numbers: 1593 and 1596). The beamforming level differences are within –0.6 and 1.3 dB for L0 and within –1.1 and 1.6 dB for L2 nozzle. They are within –1.4 and 2.1 dB for the noisy 12UH mixer with L2 nozzle at the same set point (escort numbers: 1599 and 1603). A little shift in peak locations due to slight flow condition difference is responsible for higher beamforming level difference in this case.

3.4 Effect of Venturi Nozzles

Different types of venturi nozzles are tried during the test in an attempt to reduce core and fan flow rig noise. Two core flow venturi nozzles 200B (B) and 200C (C) and a fan flow venturi 200A (A) are tested with/without a piece of one inch thick aluminum foam (F) that was installed at the exit of venturi nozzle.

Figures 3.12 and 3.13 show the narrowband spectra and beamforming results for the 12CL mixer with L0 nozzle at the set point 5000. Narrowband spectra show that the 200B with the aluminum foam (BF) is quieter than the 200C with the foam (CF) for the core flow. The aluminum foam in the bypass flow (AF) reduces noise level compared to the one without the foam (A). The beamforming level differences in Figure 3.13 show that the foam in the fan flow reduces the venturi noise. The levels in the first, second and third contour plots are between –1.8 and 8.5 dB, –3.8 and 3.9 dB, and –0.6 and 8.5 dB, respectively. The maximum of the difference levels occurs in the negative streamwise locations, indicating that the overhead array was affected by the external hardware noise from venturi and pipes.

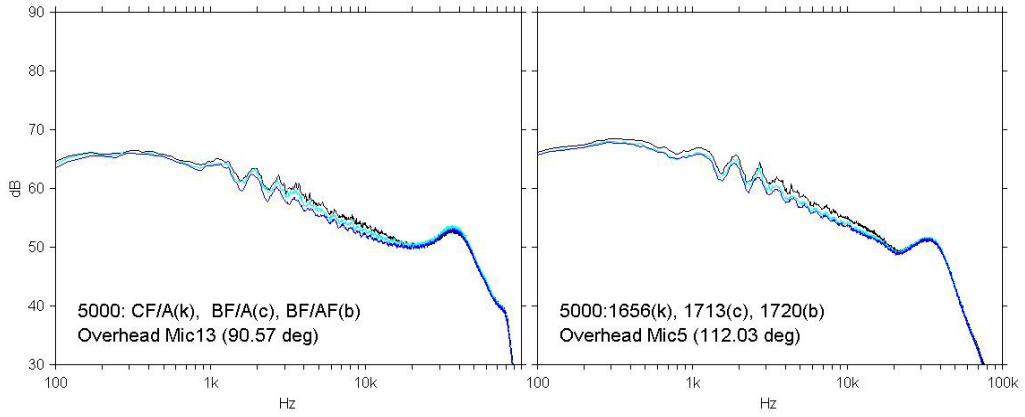

Figure 3.12.—Narrowband spectra of 12CL mixer with L0 nozzle at set point 5000 with core/fan venturi nozzles of CF/A, BF/A and BF/AF (escort numbers 1656, 1713 and 1720, respectively).

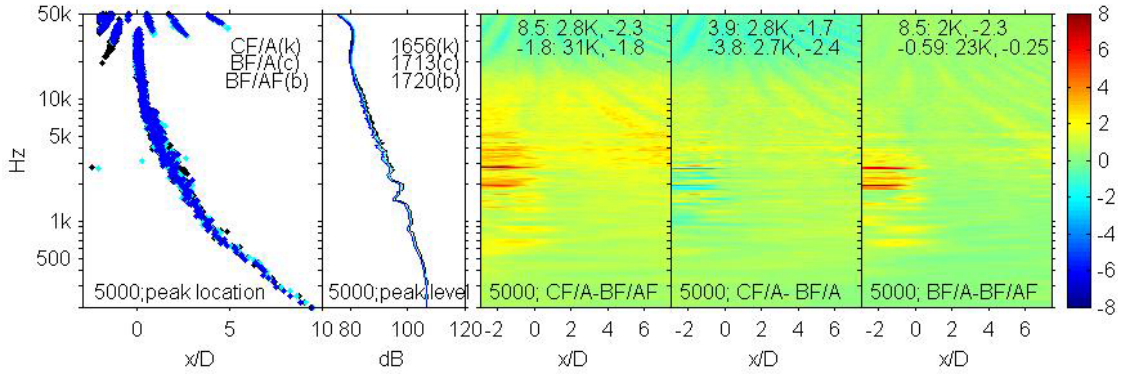

Figure 3.13.—Beamforming results of 12CL mixer with L0 nozzle at set point 5000 with core/fan venturi nozzles of CF/A, BF/A and BF/AF.

The results from the same 12CL mixer with L0 nozzle are given Figures 3.14 and 3.15 for the set points 5000, 110, and 310. The narrowband spectra are almost identical at the high speed condition 310. The foams in the core and fan flows are effective in reducing the rig noise coming out from the nozzle exit as shown in the contour plots of beamforming level differences. The foam in the bypass flow also reduces the external hardware noise at negative streamwise locations especially at low speed condition 5000. Similar results have been observed for the L1 and L2 nozzles as shown in Figures 3.16 to 3.19.

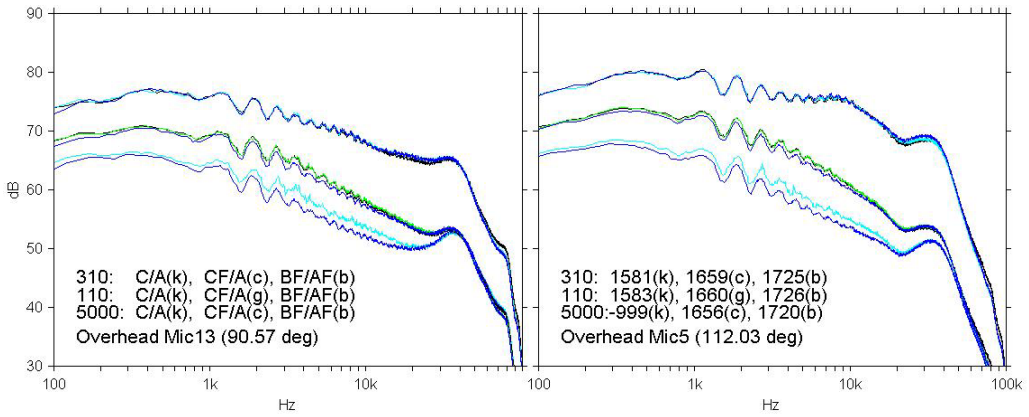

Figure 3.14.—Narrowband spectra of 12CL mixer with L0 nozzle with core/fan venturi nozzles of C/A, CF/A and BF/AF (escort numbers 1581, 1659, 1725, 1583, 1660, 1726, none, 1656, and 1720 at set points 310, 110, and 5000).

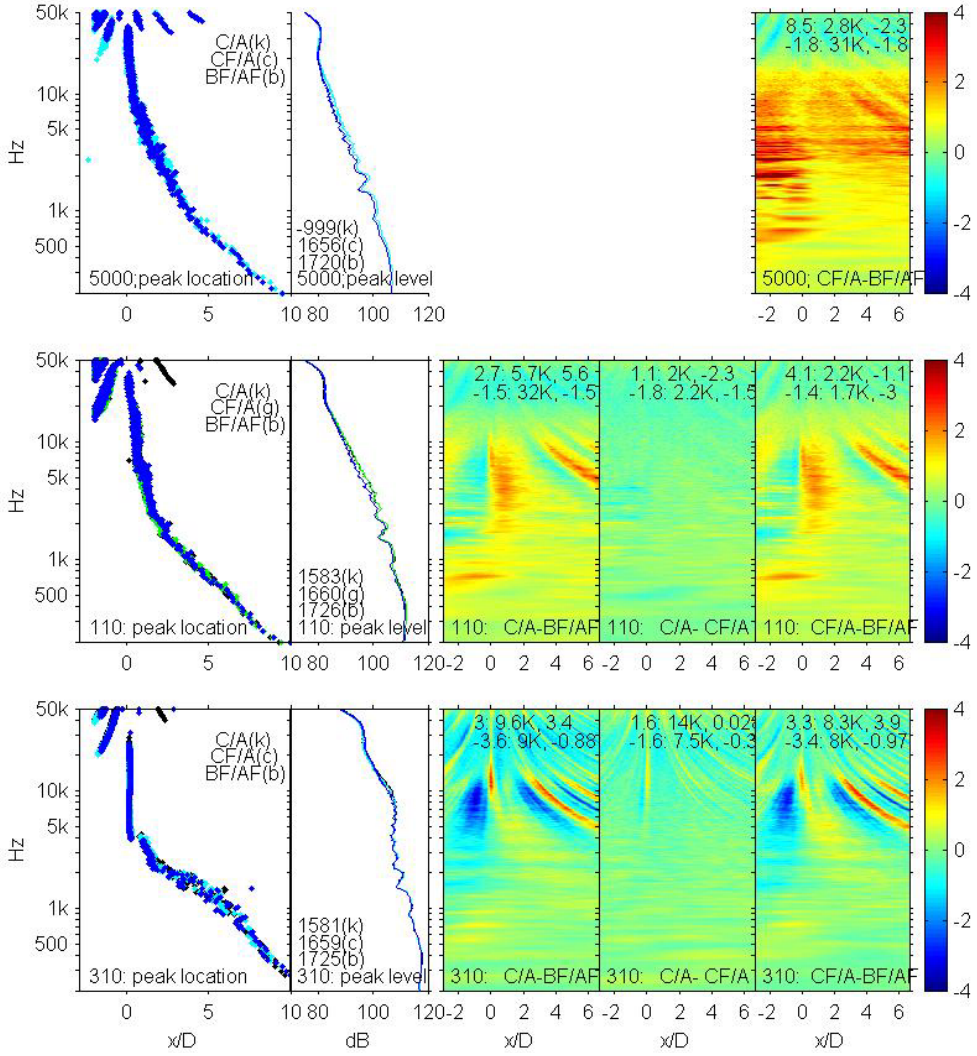

Figure 3.15.—Beamforming results of 12CL mixer with L0 nozzle with core/fan venturi nozzles of C/A, CF/A and BF/AF.

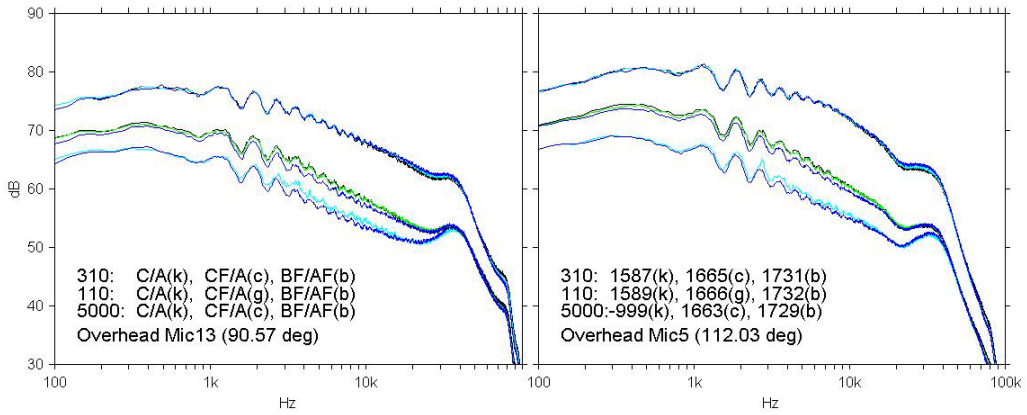

Figure 3.16.—Narrowband spectra of 12CL mixer with L1 nozzle with core/fan venturi nozzles of C/A, CF/A and BF/AF (escort numbers 1587, 1665, 1731, 1589, 1666, 1732, none, 1663 and 1729 at set points 310, 110 and 5000).

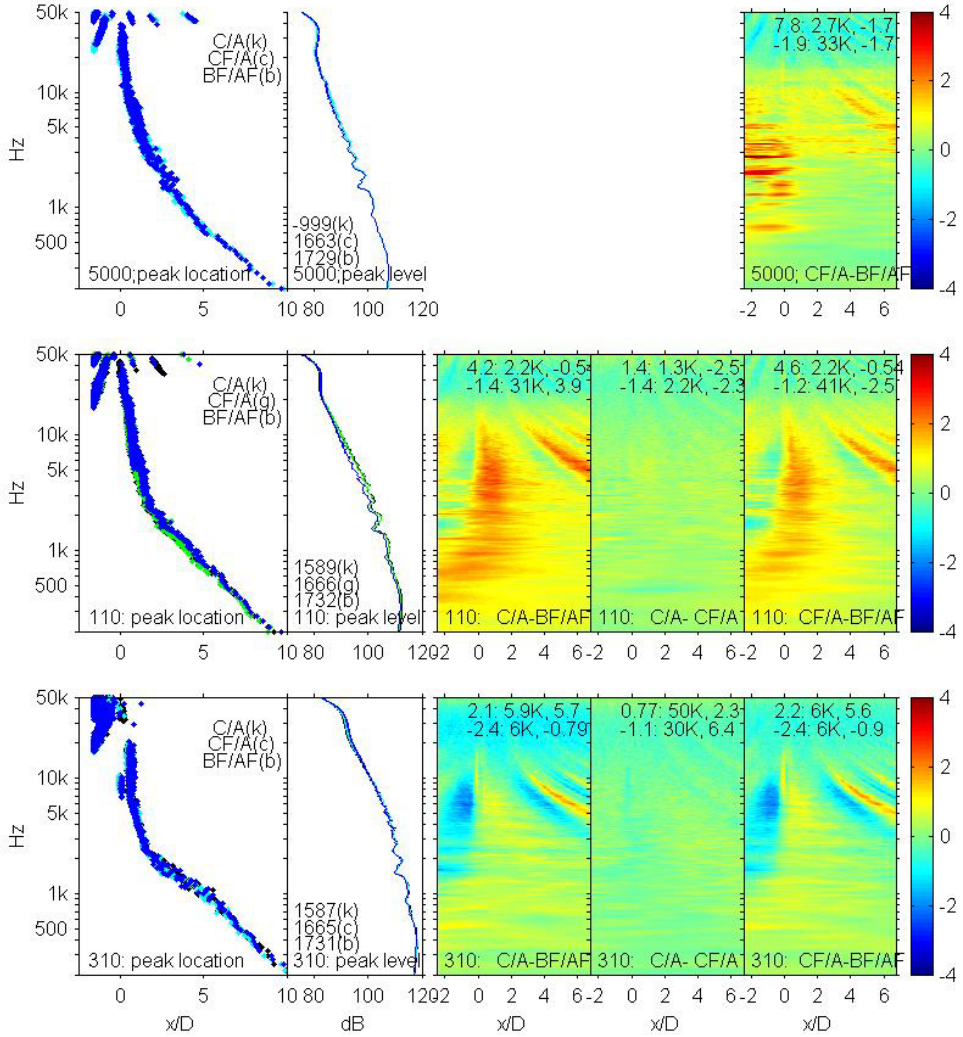

Figure 3.17.—Beamforming results of 12CL mixer with L1 nozzle with core/fan venturi nozzles of C/A, CF/A and BF/AF.

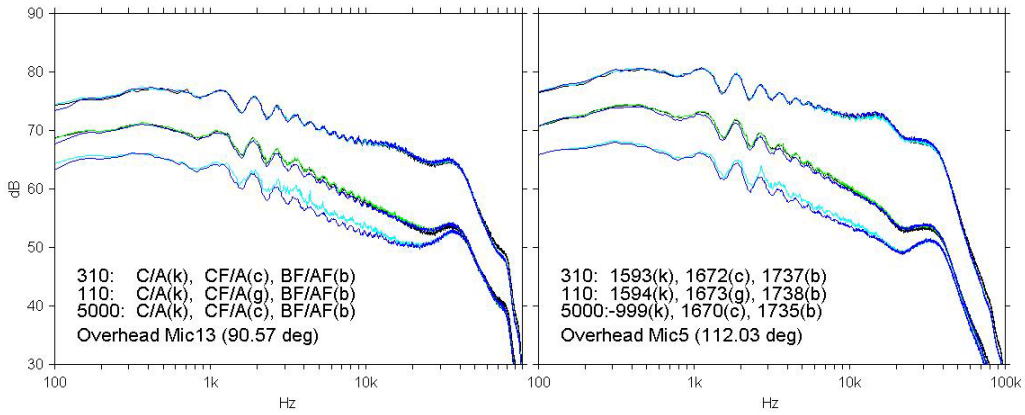

Figure 3.18.—Narrowband spectra of 12CL mixer with L2 nozzle with core/fan venturi nozzles of C/A, CF/A and BF/AF (escort numbers 1593, 1672, 1737, 1594, 1673, 1738, none, 1670, and 1735 at set points 310, 110, and 5000).

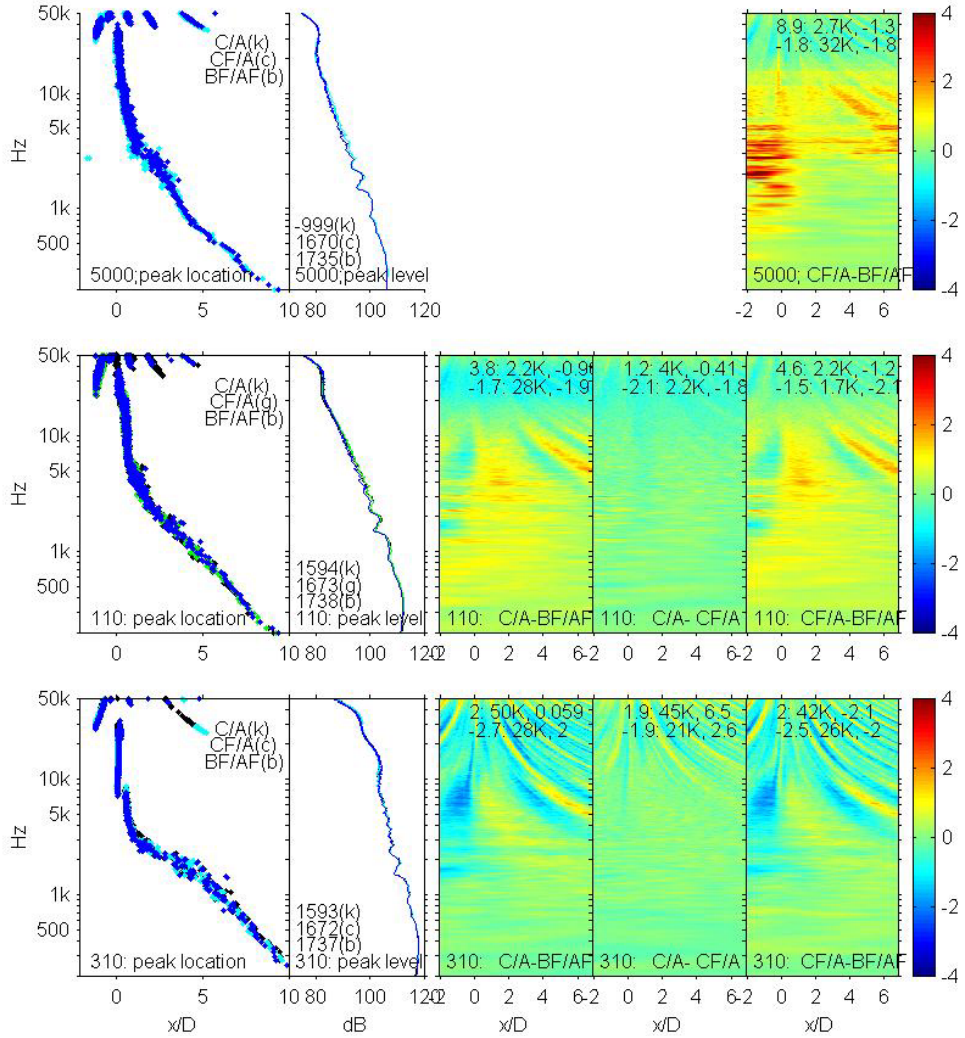

Figure 3.19.—Beamforming results of 12CL mixer with L2 nozzle with core/fan venturi nozzles of C/A, CF/A and BF/AF.

4. Effect of Nozzle

During the 1995 test it was found that the far-field spectra of lobed mixers were dependent on nozzles. Three nozzles, L0, L1 and L2 are tested with various mixers in order to understand the effect of nozzle. The L1 and L2 nozzles are 2.67 in. (0.37 diam.) and 5.43 in. (0.75 diam.) shorter than the L0 nozzle, respectively, as shown in Figure 2.1.

4.1 Effect of Nozzle on 12CL Mixer

The results of the linear phased array analyses are presented for the 12CL mixer that has the lowest penetration among three 12-lobed mixers tested in this study. Overhead array was used and the 200 °C with the aluminum foam (CF) and 200A (A) venturi nozzles are installed in the core and fan flows.

Figure 4.1 shows the narrowband spectra with the bandwidth of 24.41 Hz from the microphone numbers 13, 10, 5, and 1 of the overhead array. The corresponding microphone angles from the center of the L0 nozzle exit plane are 91°, 100°, 112°, and 128°, respectively. Since the lengths of nozzles are different and the overhead array was fixed at the same location, the microphone angles from the L1 and L2 nozzle exits are about one and two degrees larger than from the L0 nozzle. The top three lines are spectra at the set point 310 for L0(k), L1(c) and L2(r) nozzles. The lines in the middle and bottom groups are for the set points 110 and 5000, respectively. The colors of lines are given by the letters in parentheses where k, c, r, b, g and m correspond to black, cyan, red, blue, green and magenta. The humps in the spectra between 20 and 40 kHz are due to the protective grid caps on microphones.

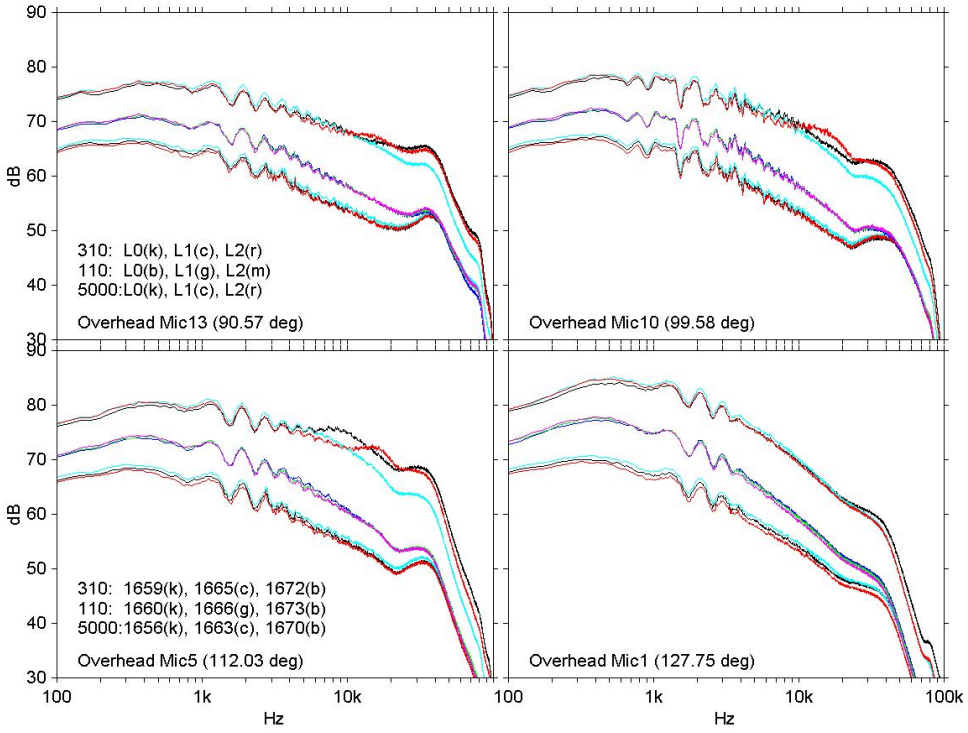

Figure 4.1.—Narrowband spectra of 12CL mixer with L0, L1 and L2 nozzles from overhead array at set points 5000, 110 and 310 (escort numbers 1656, 1663, 1670, 1660, 1666, 1673, 1659, 1665 and 1672).

At the high speed set point 310, the effect of nozzle is clearly shown in the narrowband spectra. Those of the microphone number 5 show that the medium length nozzle L1 is quieter than the other nozzles in most of frequency range. Especially, the L1 nozzle is much quieter than the longest nozzle L0 in the frequency range higher than 4 kHz and than the shortest nozzle L2 for the frequencies higher than 10 kHz. The L0 nozzle is noisier in the frequency range between 4 and 13 kHz and quieter between 13 and 22 kHz compared to the L2 nozzle. Similar behavior is found in the spectra of the upstream angle microphones 10 and 13. However, the differences are not clearly shown in the downstream microphone number 1. There is not any significant spectrum level difference between nozzles at the low speed set point 110 and the cold single jet condition set point 5000.

The results of the classical beamforming analysis are given in the top, middle and bottom rows in Figure 4.2 for the set points 5000, 110, and 310, respectively. The x coordinate is normalized by the nozzle diameter (D = 7.245 in.) and appropriately shifted so that the origin corresponds to the nozzle exit. The beamforming levels are computed along the jet centerline for all narrowband frequencies. At each frequency, the peak location and peak level are obtained at the axial location where maximum beamforming level occurs. The peak locations and peak levels are plotted in the first and second columns, where the results for the L0, L1 and L2 nozzles are plotted with black, cyan and red colors for the set points 5000 and 310 and with blue, green and magenta colors for the set point 110. In order to show the effect of nozzles on beamforming levels, the base 10 logarithms of beamforming levels for one nozzle are subtracted from those for the other nozzle. The contour plots of these beamforming level differences between the L2 and L1, L0 and L1 and L2 and L0 nozzles are given in the last three columns with corresponding color bar in dB scale. Their maximum and minimum values are printed in the figures with corresponding frequencies and x/D.

As indicated in the narrowband spectra, the nozzle effect is strongly shown at the set point 310. For the medium length nozzle L1, the peak locations change from downstream positions to nozzle exit as frequencies are increased, except between 7 and 10 kHz where the peak locations occur at the nozzle exit. The peak locations occur at about 0.5D rather than at the nozzle exit for the high frequencies between 10 and 20 kHz. In this beamforming analysis the frequencies higher than 25 kHz are not successfully resolved as peak locations incorrectly appear at sidelobe positions. The peak locations of high frequencies above 4 kHz for the longest nozzle L0 and above 8 kHz for the shortest nozzle L2 occur at the nozzle exit. It indicates that this high frequency noise was generated either inside the nozzle or at the nozzle exit. The contour plots of differences of the logarithmic beamforming levels show that the largest differences between nozzles occur at the nozzle exit.

For the low frequencies up to 4 kHz at the set point 310, the peak locations gradually vary from downstream positions to about 1D distance from the nozzle exit as frequencies are increased. This low frequency noise is due to the jet flow and the peak locations occur some distances from the nozzle exit. The L1 nozzle has higher peak levels and more upstream peak locations compared to the other nozzles. The L0 and L2 nozzles have almost identical peak locations and levels.

At the low speed set point 110, the narrowband spectra in Figure 4.1 and the peak locations and peak levels for different nozzles in Figure 4.2 show almost identical results. However, the contour plots of beamforming level differences reveal that longest nozzle L0 has higher noise level than the other two nozzles at the nozzle exit in the frequency range of 4 and 10 kHz similar to the set point 310 case.

At the set point 5000 that mimics the unheated single cold jet condition, the effect of nozzle is not significant. The external hardware noise that appears at negative x locations has been exaggerated in the contour plots since the x coordinate origin shifts are dependent on the nozzle lengths.

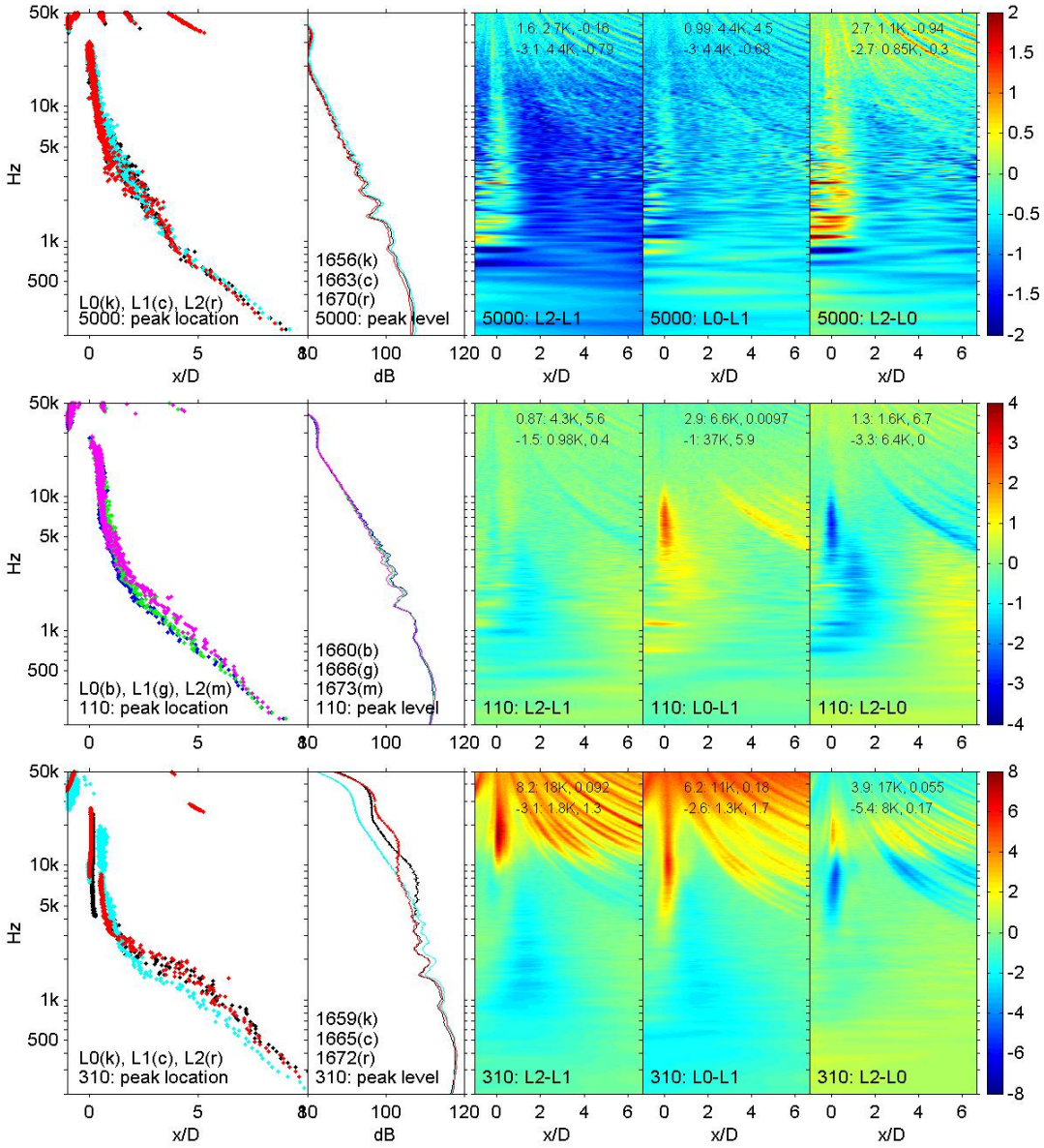

Figure 4.2.—Beamforming results of 12CL mixer with L0, L1, and L2 nozzles.

4.2 Effect of Nozzle on Confluent Splitter

Figures 4.3 and 4.4 show the effect of nozzles on the confluent splitter, Con. This axisymmetric splitter was used as a baseline for various mixer geometries. The linear array installed on the floor is used in this case. All 16 microphones are flush mounted without protective grid caps. The 200B venturi nozzle with the aluminum foam (BF) and 200A with the foam (AF) are installed in the core and fan flows. Figure 4.3 shows the narrowband spectra from the microphone numbers 3, 6, 11, and 16 whose microphone angles from the center of the L0 nozzle exit plane are 90°, 100°, 111°, and 128°, respectively. There is no L0 nozzle data at the set point 5000.

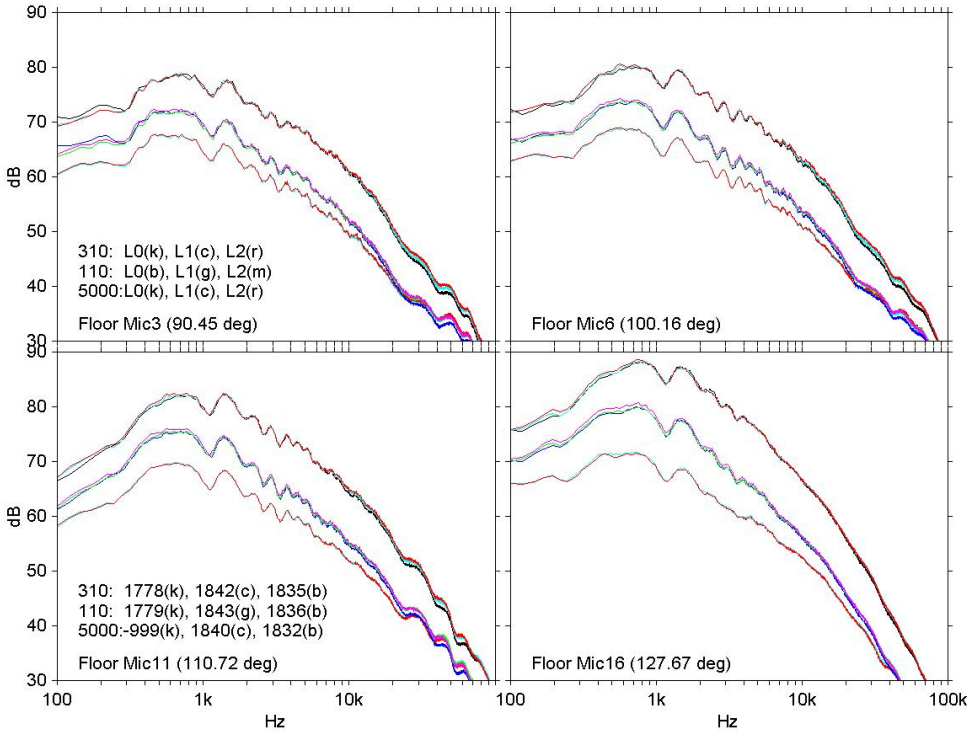

Figure 4.3.—Narrowband spectra of Confluent splitter with L0, L1, and L2 nozzles from floor array at set points 5000, 110, and 310 (escort numbers 1840, 1832, 1779, 1843, 1836, 1778, 1842, and 1835).

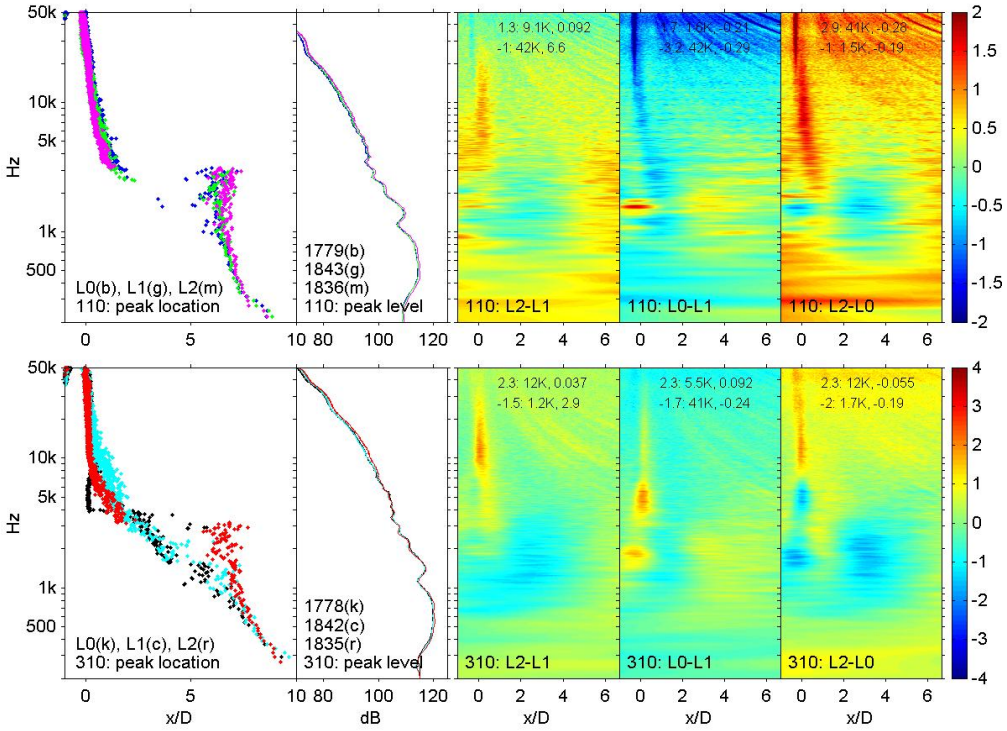

Figure 4.4.—Beamforming Results of Confluent splitter with L0, L1 and L2 nozzles.

The narrowband spectra in Figure 4.3 and the peak levels in Figure 4.4 show very little difference between nozzles. The L2 nozzle is slightly noisier than the others in the high frequency range at the set point 310. However, Figure 4.4 shows that the peak locations are dependent on nozzles at this set point. They occur at the nozzle exit for the frequencies higher than 4 kHz for the L2 nozzle and higher than 8 kHz for the L0 nozzle as in the low penetration mixer 12CL case. Although levels are much lower, the confluent splitter shows similar nozzle effect as the low penetration mixer.

4.3 Effect of Nozzle on 12UH, 20UH, and 20DS Mixers

The effect of nozzle on the highly penetrated 12-lobed mixer 12UH is shown in the narrowband spectra in Figure 4.5 and the classical beamforming results in Figure 4.6. Data were taken by the flush mounted microphones of the floor array with the 200BF and 200AF core and fan venturi nozzles. Only one nozzle was tested at the set point 5000.

At the set point 310, the spectra in Figure 4.5 and peak levels in Figure 4.6 show that the medium length nozzle L1 is the quietest and the shortest nozzle L2 is the noisiest in almost all frequency range. The L1 nozzle is quieter than L2 and L0 for the frequencies higher than 3 and 10 kHz, respectively. This is consistent with the results of the low penetration mixer 12CL given in Figures 4.1 and 4.2. The longest nozzle L0 is quieter than the L2 nozzle in most frequency range in contrast to the 12 CL mixer case where the former is quieter or noisier than the latter depending on the frequency ranges. The results of the 12UH mixer are similar to those of the 20UH and 20DS mixers given in Figures 4.8 and 4.10.

It is also shown that the L2 nozzle is noisier than the other two nozzles at the low speed set point 110. The peak levels for L0 and L1 are almost identical. At this set point, the spectrum level differences between nozzles are larger for the 12UH, 20UH and 20DS mixers than for the confluent splitter and 12CL mixer.

The effect of nozzles on peak locations of this noisy mixer is less than in the low penetration mixer 12CL and the confluent splitter shown in Figures 4.2 and 4.4. However, it is observed that the high frequency peak locations of the L0 and L2 nozzles occur closer to the nozzle exit compared to the L1 nozzle at both set points 110 and 310. It is interesting to note that the high frequency peak locations actually occur a little upstream of nozzle exit at the set point 310 for the L0 and L2 nozzles. Similar results are found in the 20UH and 20DS mixers.

Beamforming results from the overhead linear phased-array are very similar to those from the floor array given in Figure 4.6. Since the microphone positions of the floor array have been accurately measured, the floor array was able to handle up to very high frequencies compared to the overhead array whose high frequency limit was about 25 kHz.

The results of the 20-lobed mixers 20UH and 20DS from overhead array, given in Figures 4.7 to 4.10, are similar to the 12UH mixer case. The 200CF/200A for the 20DS and 20UH with L2 nozzle and 200C/200A for 20UH with L0 and L1 nozzles are used for the core/fan venturi nozzles. The beamforming level differences between the L2 and other nozzles are larger in these 20-lobed mixers than in the 12-lobed 12UH mixer.

For all tested mixers, including confluent splitter and 12CL, 12UH, 20UH and 20DS mixers, big difference of the beamforming levels between nozzles occurs at the nozzle exit. These results show that the high frequency noise, of higher than 3 or 4 kHz, is strongly dependent on the nozzle geometry. Among the three nozzles tested, the medium length nozzle L1 was the quietest for all mixers. The nozzle effect is stronger at the high speed set point 310 than at the low speed set point 110. At the high speed set point both spectrum levels and peak locations are very much dependent on the nozzles.

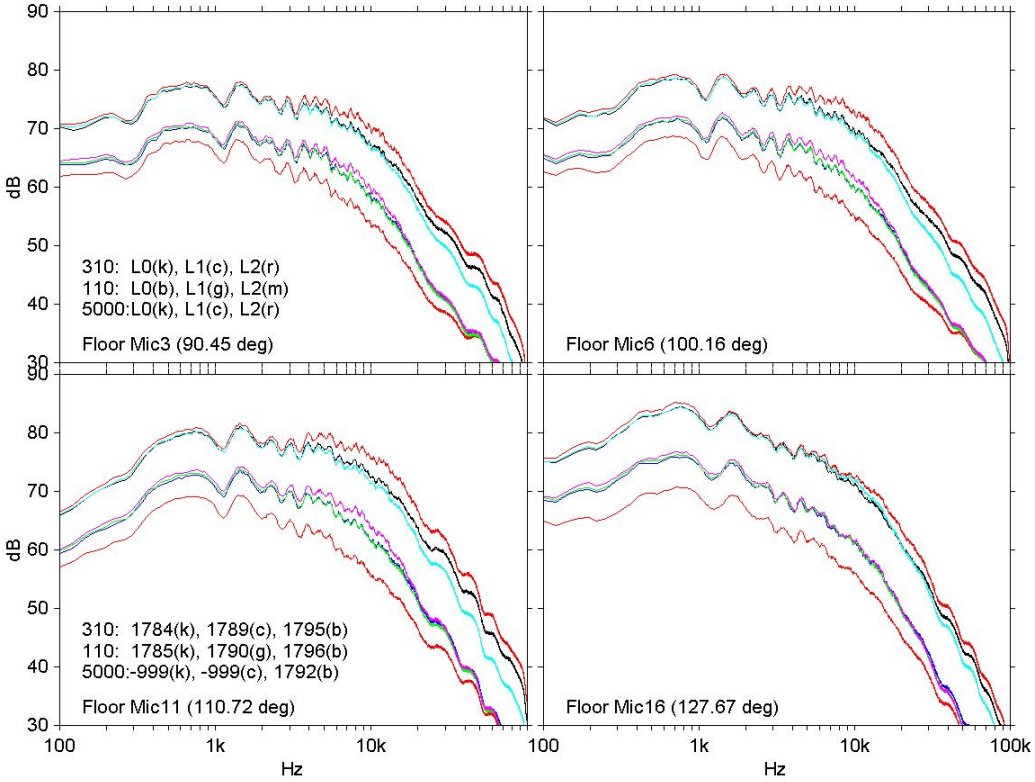

Figure 4.5.—Narrowband spectra of 12UH mixer with L0, L1 and L2 nozzles from floor array at set points 5000, 110, and 310 (escort numbers 1792, 1785, 1790, 1796, 1784, 1789, and 1795).

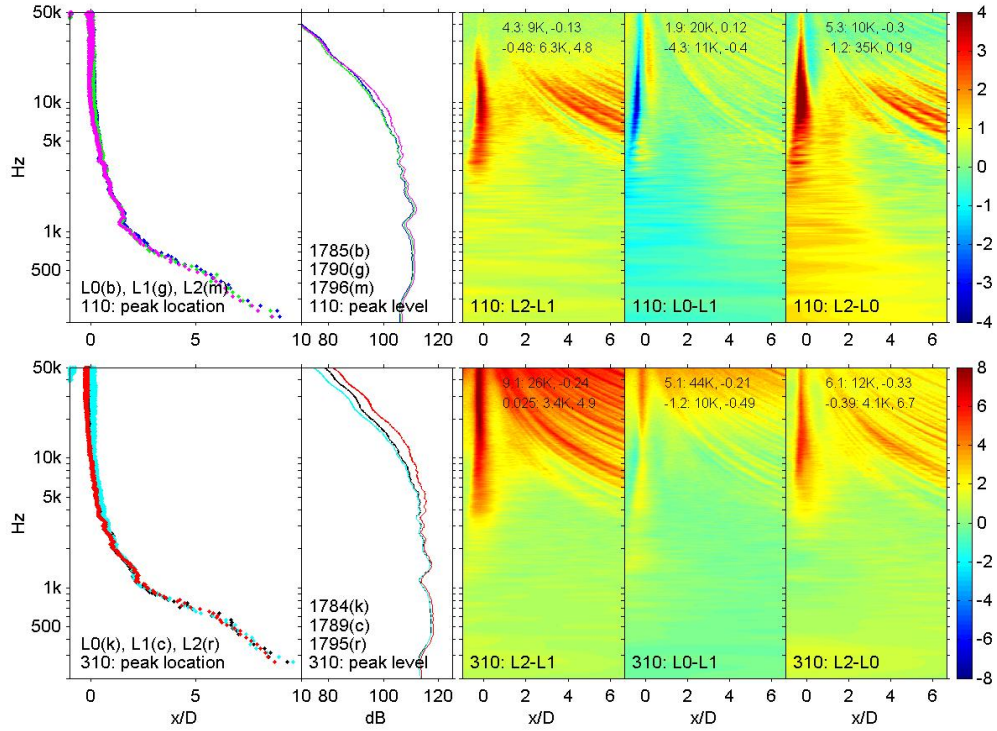

Figure 4.6.—Beamforming results of 12UH mixer with L0, L1 and L2 nozzles.

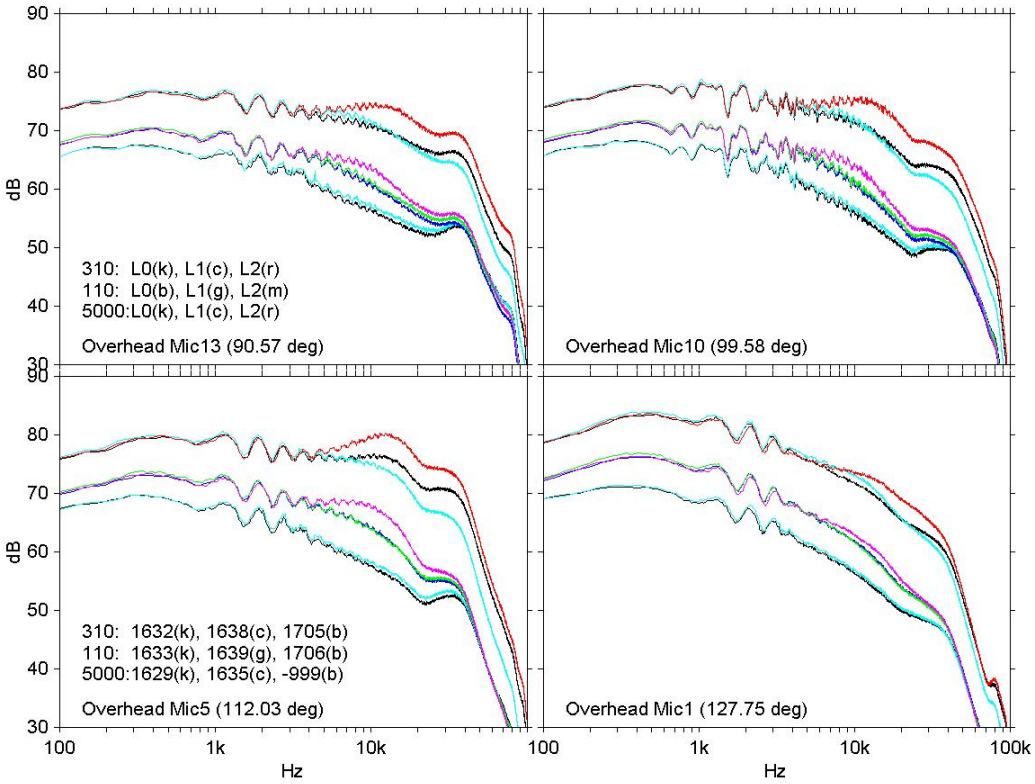

Figure 4.7.—Narrowband spectra of 20UH mixer with L0, L1, and L2 nozzles from overhead array at set points 5000, 110, and 310 (escort numbers 1629, 1635, 1633, 1639, 1706, 1632, 1638, and 1705).

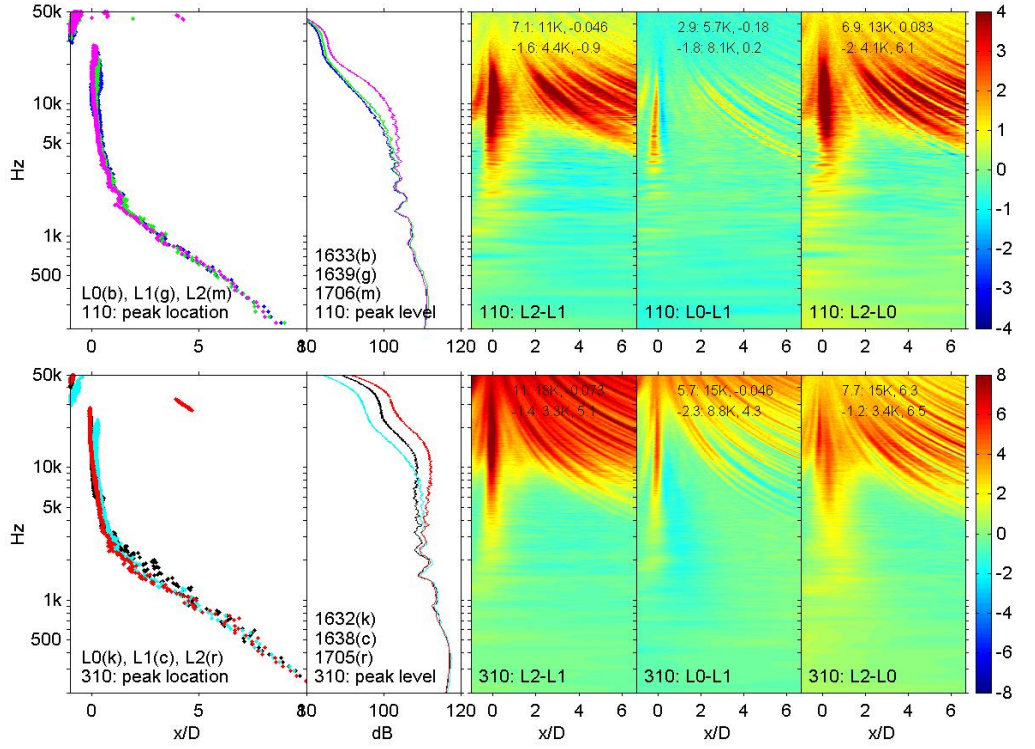

Figure 4.8.—Beamforming results of 20UH mixer with L0, L1, and L2 nozzles.

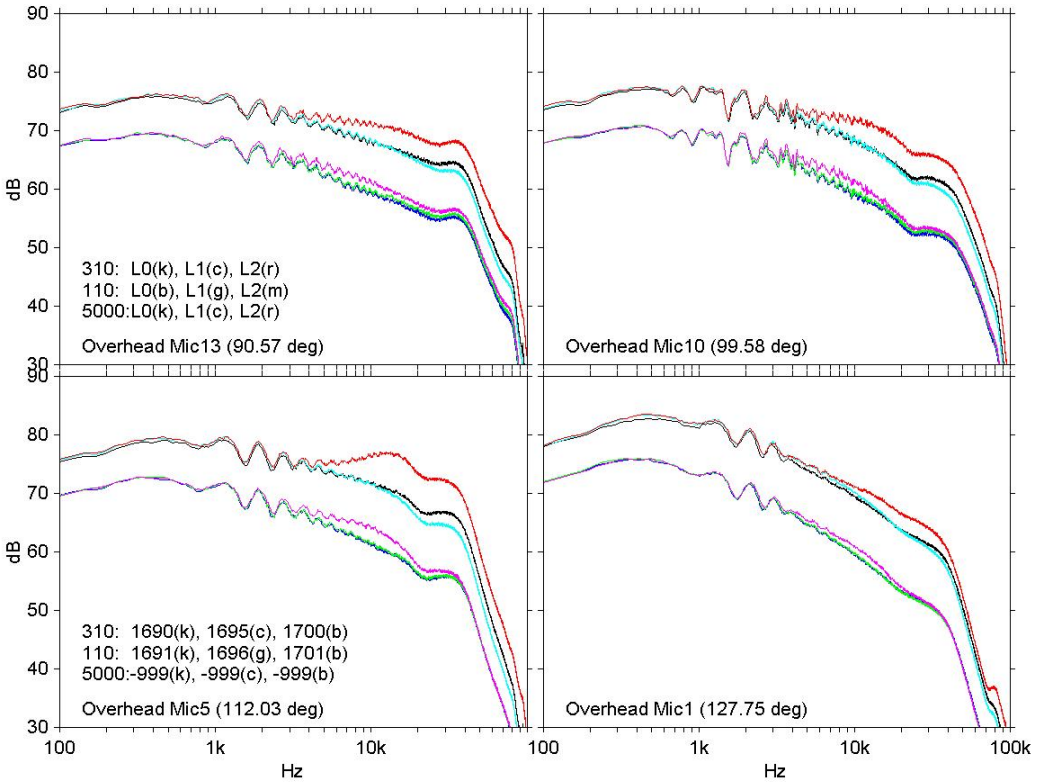

Figure 4.9.—Narrowband spectra of 20DS mixer with L0, L1, and L2 nozzles from overhead array at set points 5000, 110, and 310 (escort numbers 1691, 1696, 1701, 1690, 1695, and 1700).

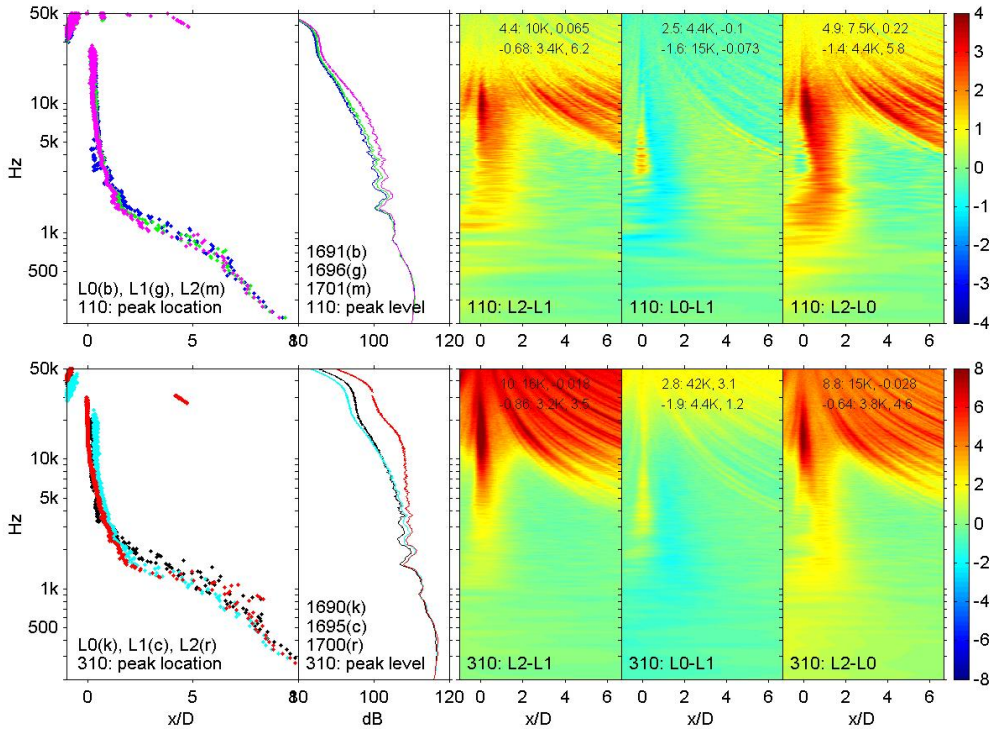

Figure 4.10.—Beamforming results of 20DS mixer with L0, L1, and L2 nozzles.

5. Effect of Mixer

The phased-array analyses of the effect of mixer will be presented in this section. The confluent splitter, three 12-lobed mixers, 12CL, 12UM, and 12UH, and two 20-lobed mixers 20UH and 20DS are tested. The confluent axisymmetric splitter is served as baseline configuration. The 12CL, 12UM, and 12UH mixers have low, medium and high peak to peak penetrations of 0.5, 0.7, and 0.88 of the mixer plane annulus, respectively, as shown in Figure 4.2. The 20UH and 20DS mixers have the same high penetration as the 12UH mixer. The 20DS mixer has deep scallops.

5.1 Effect of Mixer on L1 Nozzle

It was shown in the previous section that the medium length nozzle L1 is the quietest among the three nozzles tested.

Figures 5.1 and 5.2 show the narrowband spectra and beamforming results of the confluent splitter and the 12-lobed high penetration mixer 12UH with the L1 nozzle by using the floor array. As shown in the spectra of the microphone number 11, the 12UH mixer reduced low frequency but increased high frequency noise with crossing frequencies at about 1.5 and 2 kHz at the set points 110 and 310, respectively. The peak levels obtained from the classical beamforming method show the same behavior. The peak locations of the 12UH mixer occur at more upstream positions compared to the confluent splitter for all frequencies. The contour plots of beamforming level difference show that the added high frequency noise of the 12UH mixer occurs at or close to the nozzle exit. This indicates that small scale turbulence enhanced by the mixer increased the level of this high frequency noise.

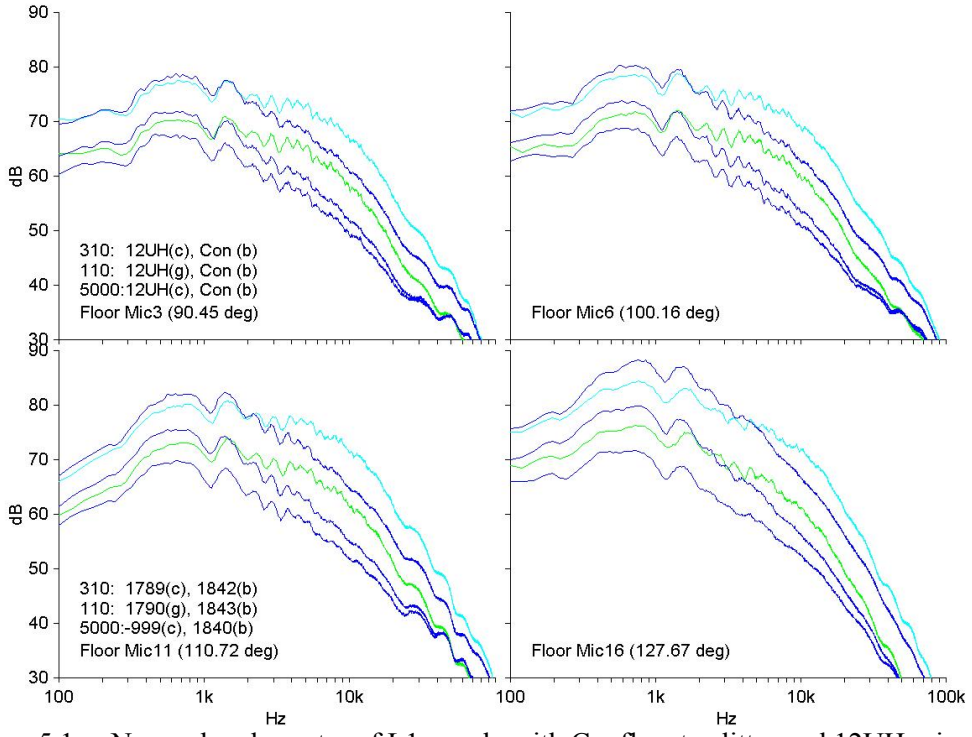

Figure 5.1.—Narrowband spectra of L1 nozzle with Confluent splitter and 12UH mixer from floor array at set points 5000, 110, and 310 (escort numbers 1840, 1790, 1843, 1789, and 1842).

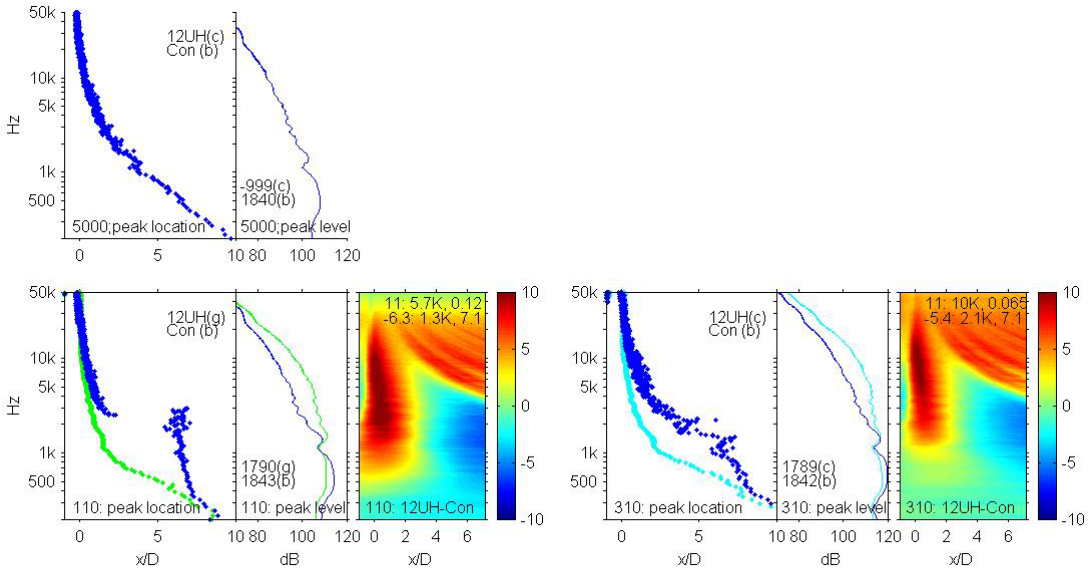

Figure 5.2.—Beamforming results of L1 nozzle with Confluent splitter and 12UH mixer.

The narrowband spectra and the beamforming results are given in Figures 5.3 and 5.4 where the L1 nozzle was tested with the 12CL, 12UH, 20UH, and 20DS mixers by using the overhead array.

The comparison between the low and high penetration 12-lobed mixers, 12CL and 12UH shows that the spectrum levels of the 12UH mixer are a little lower than the 12CL mixer in low frequency ranges. However, when the frequencies are higher than 1 and 1.5 kHz at the set points 110 and 310, respectively, the noise levels of the 12UH mixer is much higher than the 12CL mixer. In fact, in these high frequency ranges the 12-lobed mixer 12UH is noisier than the other 20-lobed mixers 20UH and 20DS of the same penetration. The contour plots of the beamforming level differences reveal that the 12UH mixer produces much higher noise near the nozzle exit then the 12CL mixer for the frequencies higher than 500 Hz and 1 kHz at the set points 110 and 310, respectively. It is shown in Figure 5.4 that the 12UH mixer has the most upstream peak locations and highest peak levels among all four mixers.

By comparing the results of the 20UH and 12UH mixers, we can show that high frequency noise can be reduced by reducing the width of lobe or by increasing lobe number. The 20-lobed 20UH mixer has lower spectrum levels than the 12-lobed 12UH mixer in the high frequency range above about 1 or 1.5 kHz. The low frequency noise of the 20UH mixer was slightly increased. The spectrum levels of the 20UH mixer are in between those of the 12UH and 12CL mixers. Figure 5.4 shows that most of the peak level reductions between the 20UH and 12UH mixers occur in the frequency range between 1 and 6 kHz. The contour plots of beamforming level differences between 12UH and 20UH, 12UH and 12CL, and 20UH and 12CL show that the most noise reduction occurs near the nozzle exit.

Introducing a deep scallop was very successful in reducing mixer noise. The narrowband spectrum levels of the 20-lobed high penetration mixer with deep scallop, 20DS are lower than the 20UH and 12UH mixers in all frequencies at both set points 110 and 310. The spectrum levels from 112° microphone show that the 20DS mixer is much quieter than the low penetration mixer 12CL in the low frequency ranges below 5 and 10 kHz at the 110 and 310 set points, respectively. The penalty at higher frequency is relatively small especially at the high speed set point 310. The contour plots in Figure 5.4 confirm that the 20DS mixer is quieter than the 12UH and 20UH mixers in almost all grid points that cover from -1D to 7D streamwise locations and from 200 Hz to 50 kHz frequencies. The 20DS mixer is also quieter than the 12CL mixer in downstream locations and low frequencies, though it is a little noisier at higher frequencies near the nozzle exit.

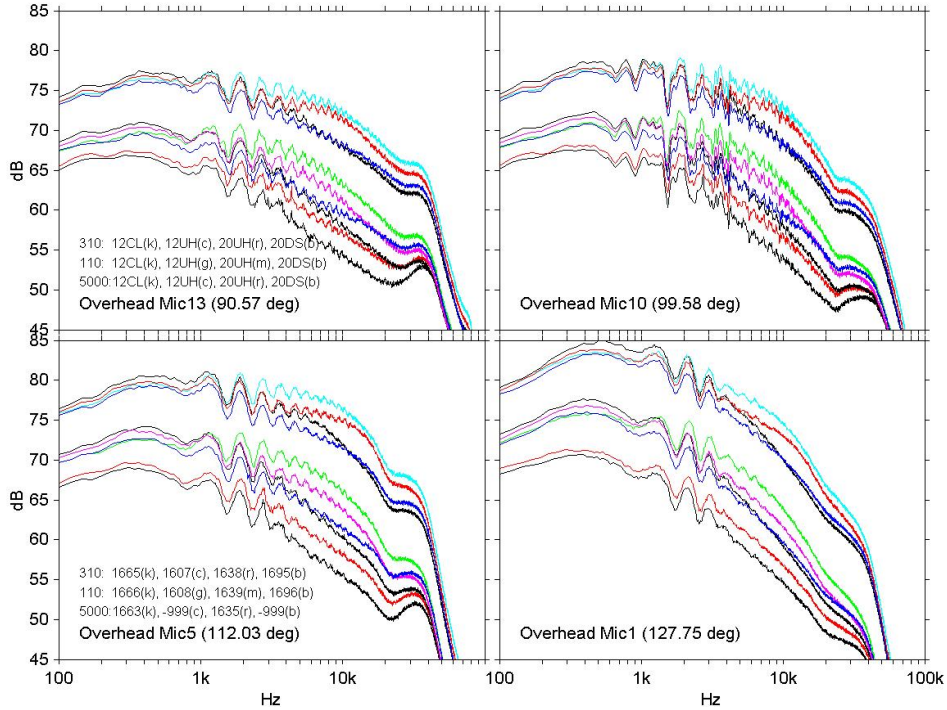

Figure 5.3.—Narrowband spectra of L1 nozzle with 12CL, 12UH, 20UH and 20DS mixers from overhead array at set points 5000, 110, and 310 (escort numbers 1663, 1635, 1666, 1608, 1639, 1696, 1665, 1607, 1638, and 1695).

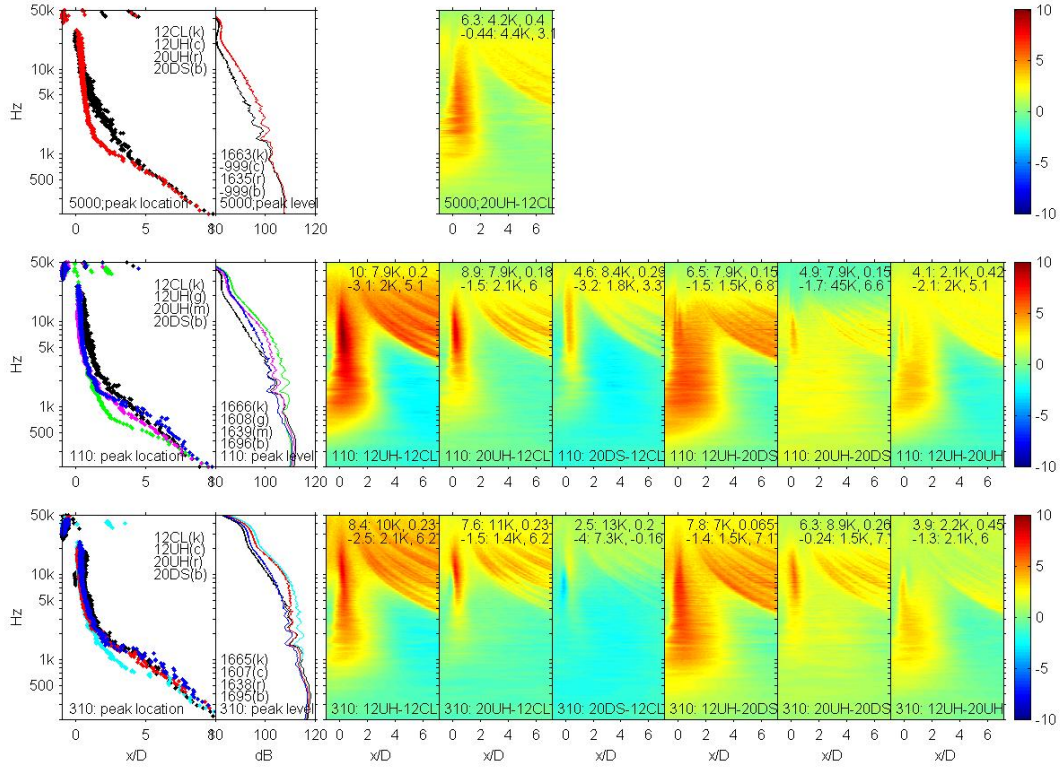

Figure 5.4.—Beamforming results of L1 nozzle with 12CL, 12UH, 20UH and 20DS mixers.

5.2 Effect of Mixer on L2 Nozzle

The L2 nozzle is the shortest one tested. The previous results show that this is noisier than the L1 nozzle especially near the nozzle exit. The narrowband spectra and beamforming results of the confluent splitter and the 12CL and 12UH mixers from the floor array are given in Figures 5.5 and 5.6. The overhead array results of the 12CL, 12UH, 20UH, and 20DS mixers are shown in Figures 5.7 and 5.8.

The general trends are similar to the L1 nozzle case discussed in the previous section. For example, the spectrum level from the 111° floor microphone in Figure 5.5 shows that the level of the 12UH mixer is higher than the confluent splitter for the frequencies higher than 1.5 kHz.

Difference between this and the quietest L1 nozzle occurs at high frequencies where the former is noisier than the latter. Comparing Figure 5.7 against Figure 5.3, we can show that the high frequency noise level difference between the 20DS and 12CL mixers for the L2 nozzle is much larger than that for the L1 nozzle. The contour plots in Figures 5.6 and 5.8 show that, at the frequencies higher than about 6 or 10 kHz at the high speed set point 310, the L2 nozzle with high penetration mixers, 12UH, 20UH, and 20DS is much noisier at the nozzle exit than with the low penetration mixer 12CL.

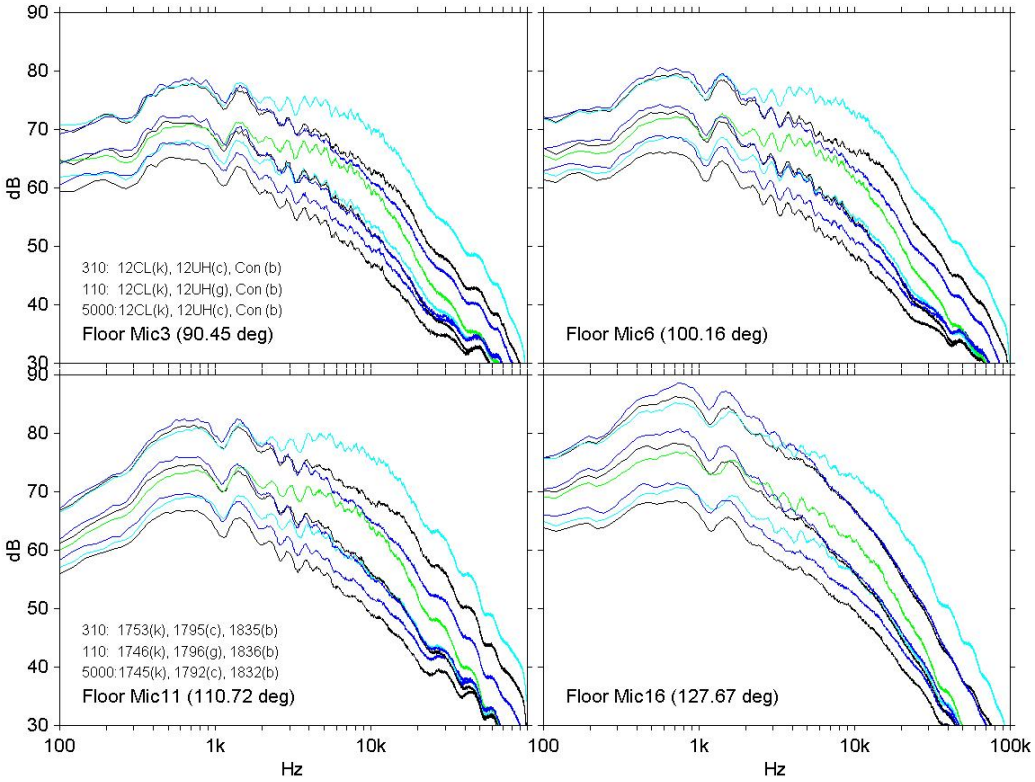

Figure 5.5.—Narrowband spectra of L2 nozzle with Con, 12CL and 12UH mixers.

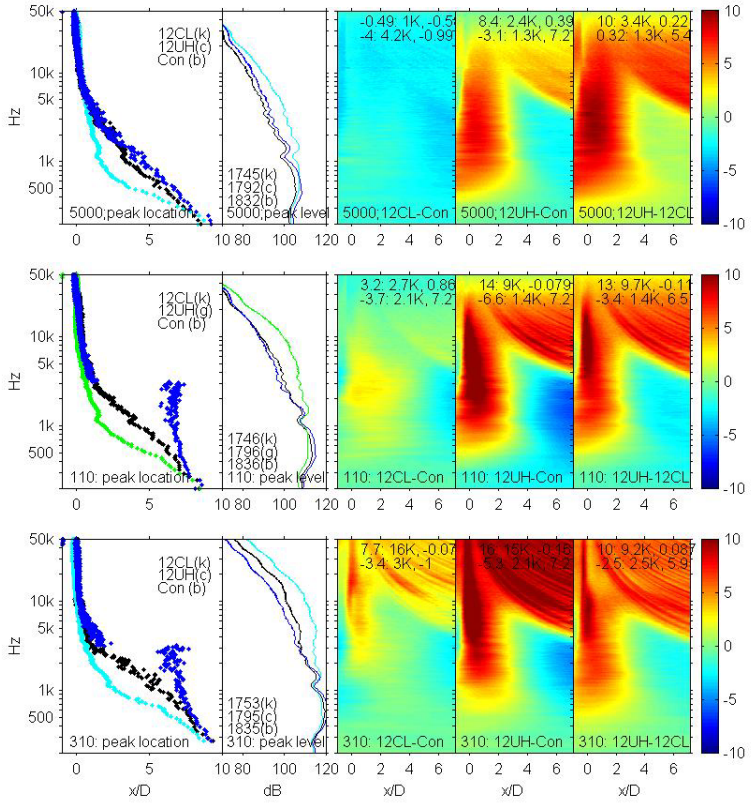

Figure 5.6.—Beamforming results of L2 nozzle with Con, 12CL and 12UH mixers.

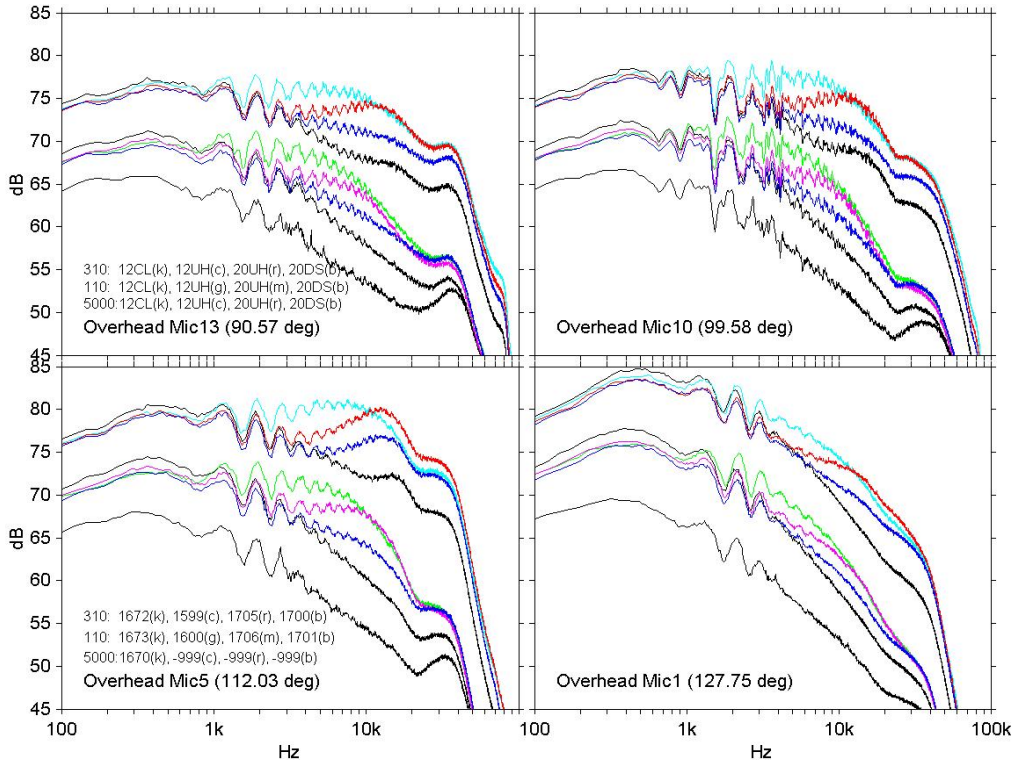

Figure 5.7.—Narrowband spectra of L2 nozzle with 12CL, 12UH, 20UH and 20DS mixers.

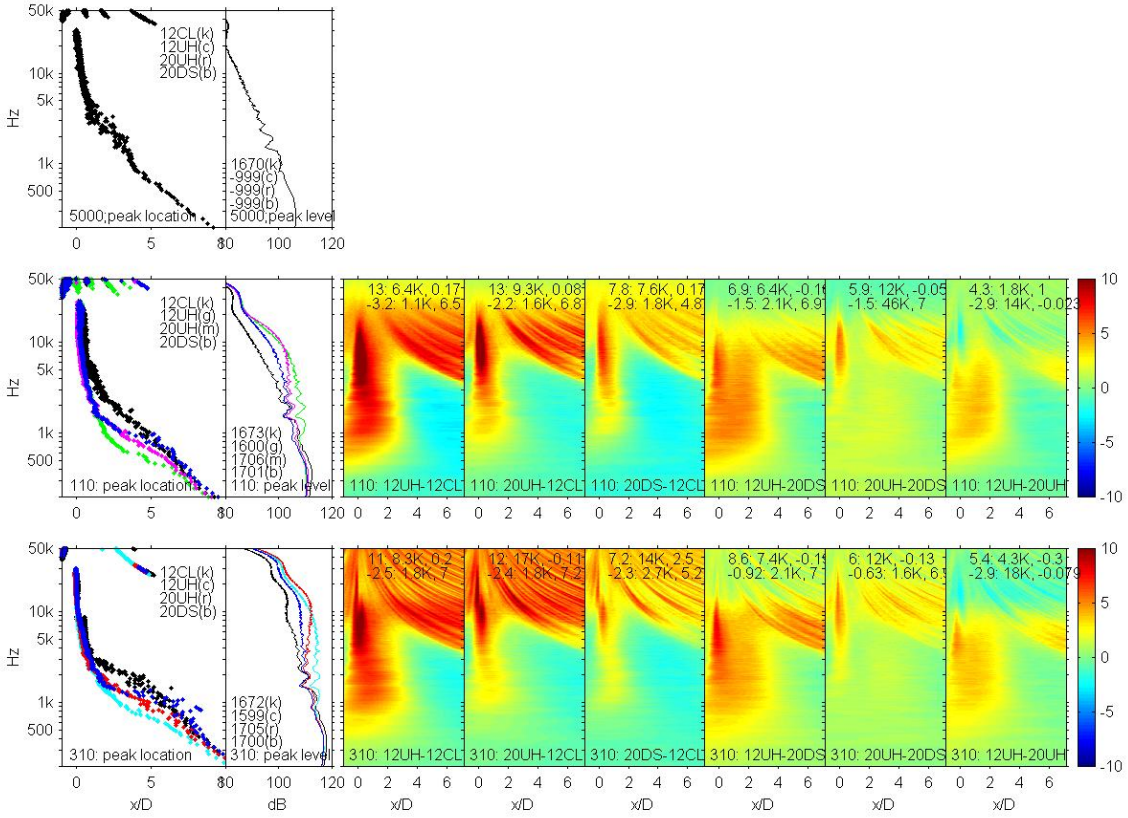

Figure 5.8.—Beamforming results of L2 nozzle with 12CL, 12UH, 20UH and 20DS mixers.

5.3 Effect of Mixer on L0 Nozzle

It is shown in the previous chapter that the longest L0 nozzle generates higher high frequency noise at the nozzle exit compared to the L1 nozzle. The floor array results for the confluent splitter and the 12UH mixer given in Figures 5.9 and 5.10 and overhead array results for the 12CL, 12UH, 20UH and 20DS mixers given in Figures 5.11 and 5.12 show similar behaviors observed in the L1 and L2 nozzle cases. The effect of the high frequency noise at the nozzle exit is shown in the contour plots in Figures 5.10 and 5.12.

Figures 5.13 and 5.14 show the narrowband spectra and beamforming results from the overhead array for the 12CL, 12UH, and 12UM and confluent splitter. The noise level of the medium penetration mixer 12UM is in between those of the 12CL and 12UH mixers. In general, at all set points 5000, 110, and 310, the noise level of the 12UM mixer is lower than the 12UH mixer in high frequency range and lower than the 12CL mixer in low frequencies. The spectra from 112° microphone, in Figure 5.13 show that this medium penetration mixer has the highest spectrum level at about 10 kHz at the set point 310.

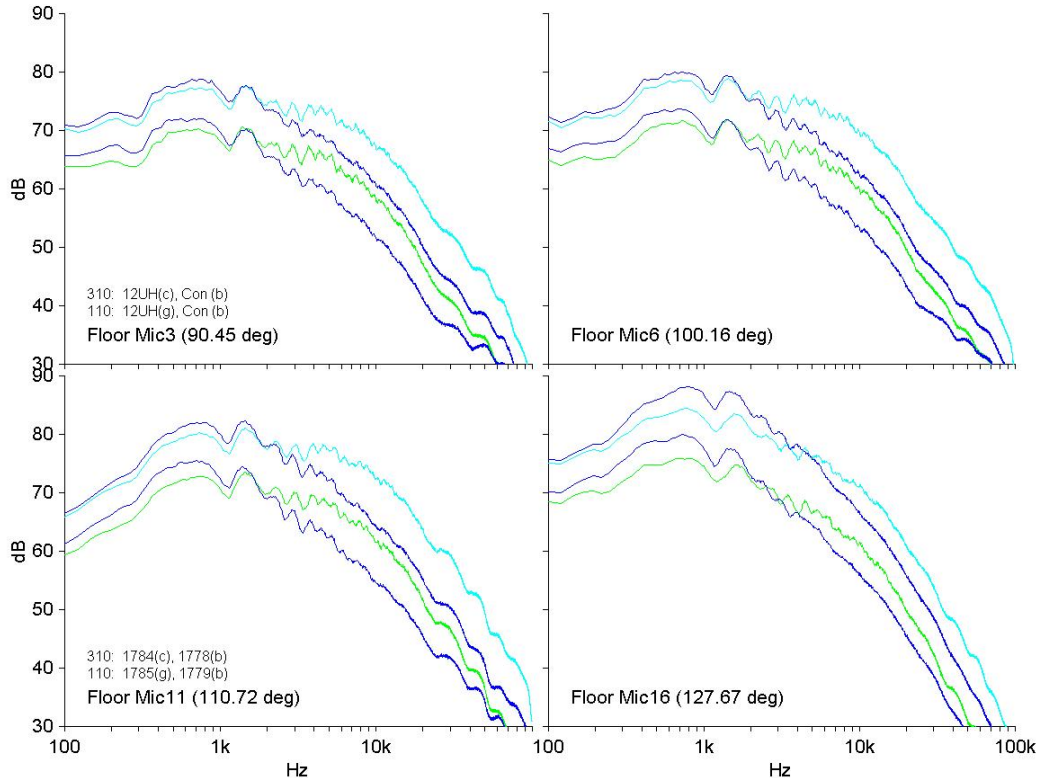

Figure 5.9.—Narrowband spectra of L0 nozzle with Confluent splitter and 12UH mixer.

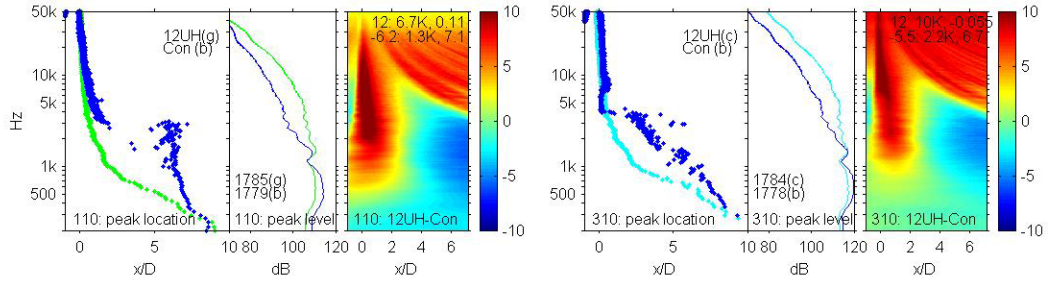

Figure 5.10.—Beamforming results of L0 nozzle with Confluent splitter and 12UH mixer.

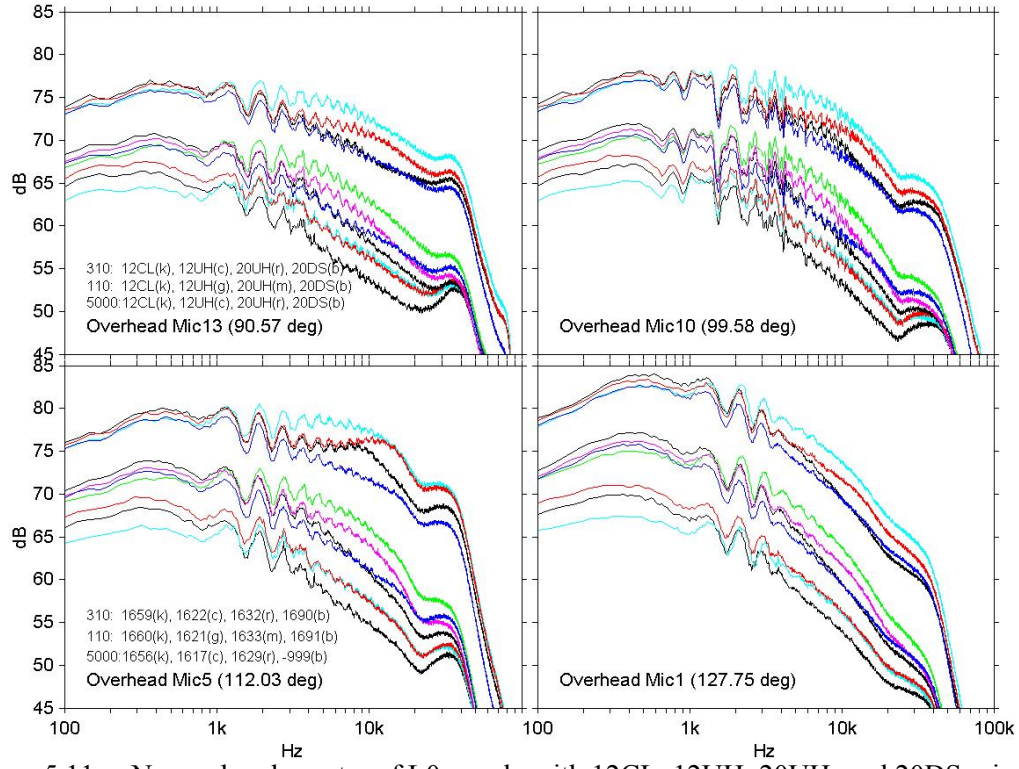

Figure 5.11.—Narrowband spectra of L0 nozzle with 12CL, 12UH, 20UH, and 20DS mixers.

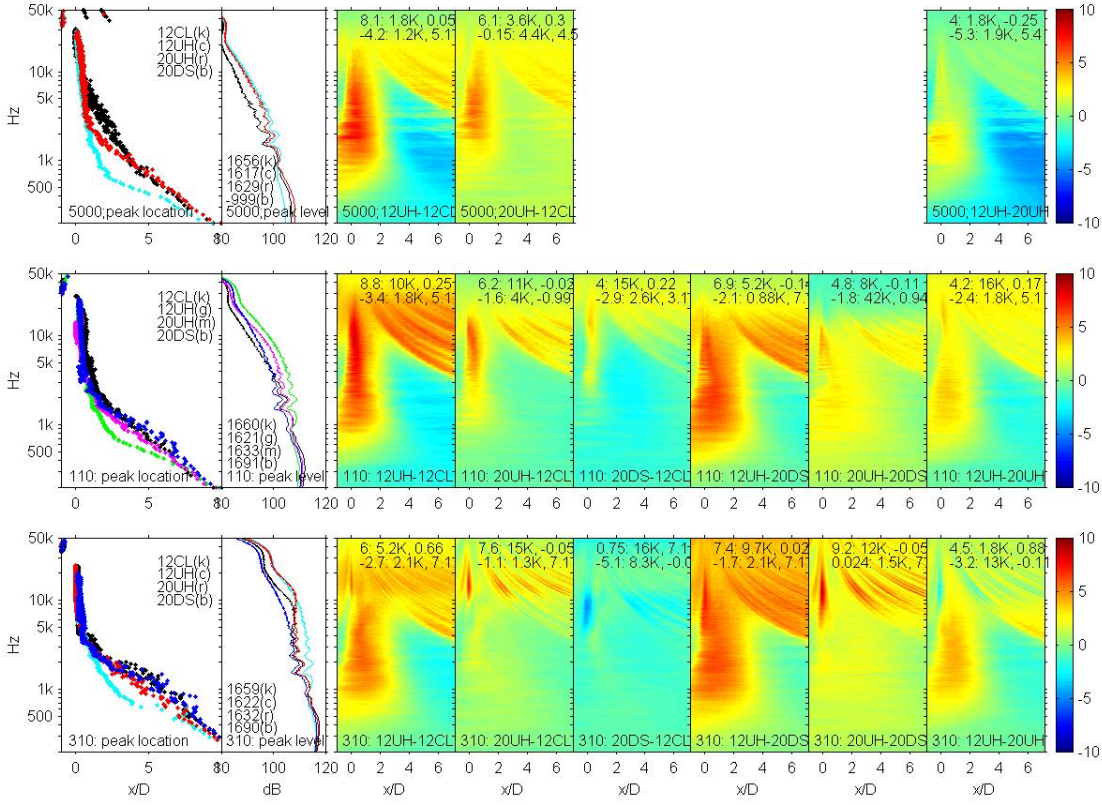

Figure 5.12.—Beamforming results of L0 nozzle with 12CL, 12UH, 20UH, and 20DS mixers.

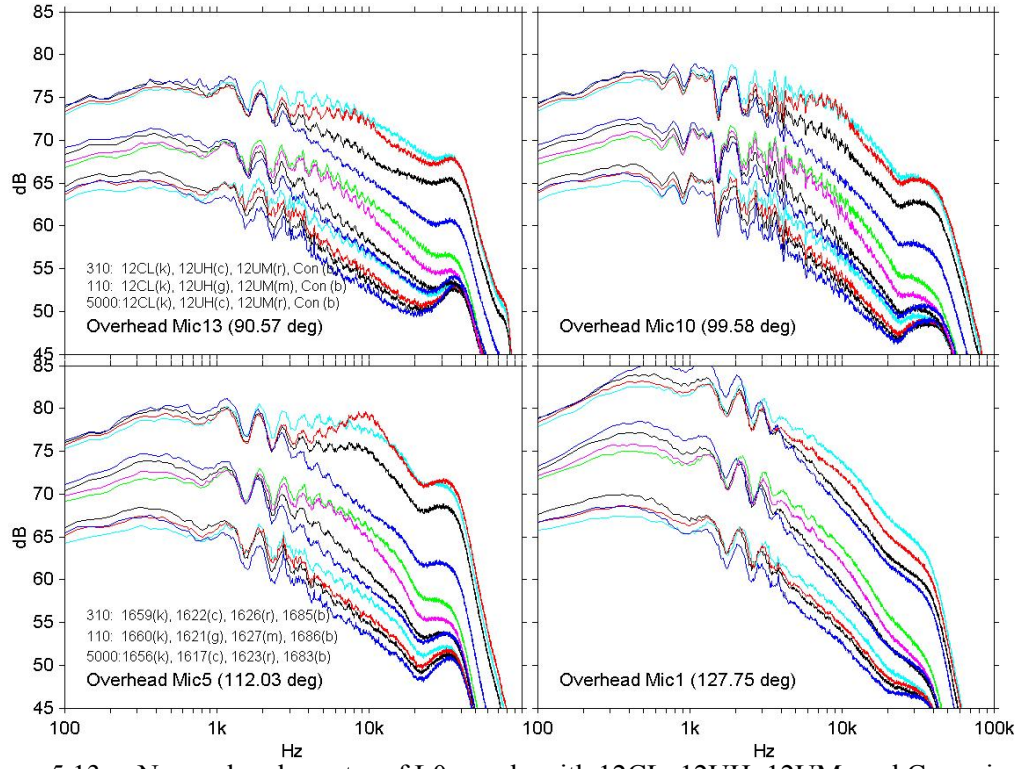

Figure 5.13.—Narrowband spectra of L0 nozzle with 12CL, 12UH, 12UM, and Con mixers.

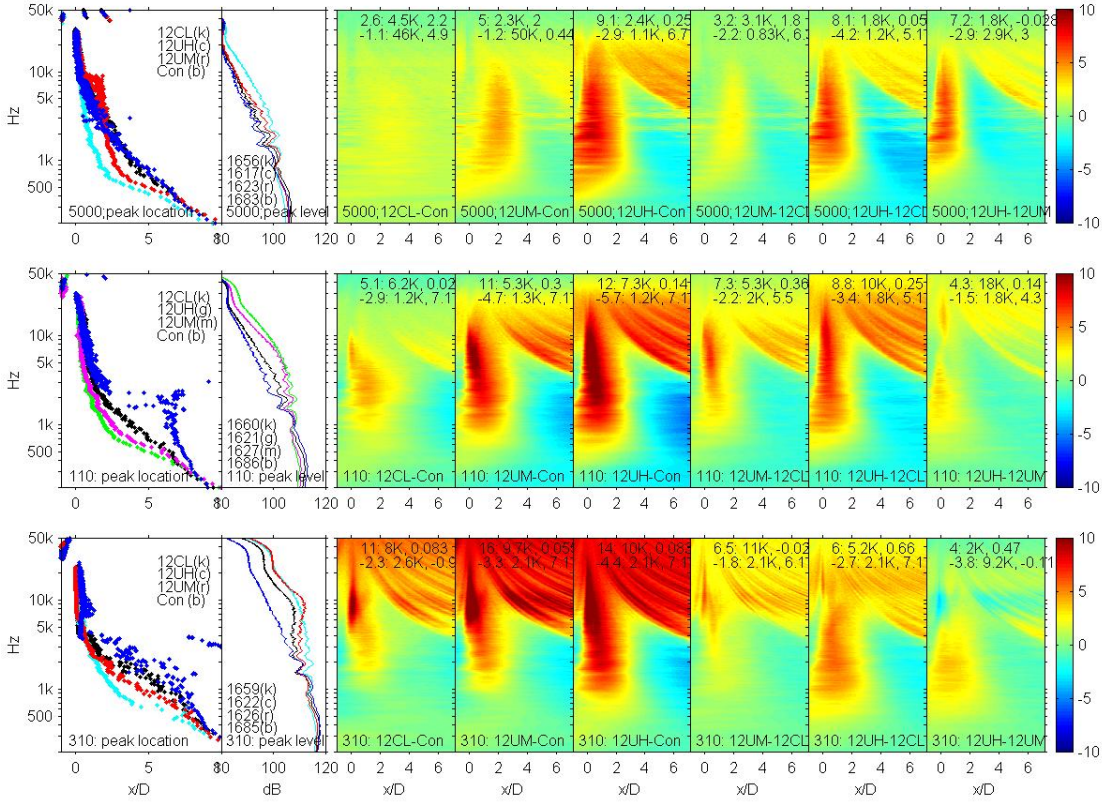

Figure 5.14.—Beamforming results of L0 nozzle with 12CL, 12UH, 12UM, and Con mixers.

6. Concluding Remarks

The phased-array system has been successfully applied to identify the noise source locations. It was shown that the 16 microphone linear phased-array system installed in parallel with the jet-flow centerline, could detect correct source locations.

In general, the high frequency jet noise was coming from near the nozzle exit and the low frequency noise was coming from near the end of the potential core. The source locations are smoothly varying from the nozzle exit to the end of potential core as the frequencies decrease at the flow condition 5000 that mimics single flow jet. The frequency-source location dependency is not smooth at the other flow conditions because mixer and nozzle altered the flow field from that of a single flow jet. The various mixers and nozzles increase/decrease noise of certain frequency components and the phased-array beamforming can find the locations of the added noise sources. It was also able to detect any internal rig noise that is shown to be coming right from the nozzle exit.

For all mixers, confluent splitter and 12CL, 12UH, 20UH, and 20DS mixers, big difference of the beamforming levels between nozzles occurs at the nozzle exit. The high frequency noise, of higher than 3 or 4 kHz, is strongly dependent on the nozzle geometry. Among the three nozzles tested, the medium length nozzle L1 was the quietest for all mixers. The nozzle effect is stronger at the high speed set point 310 than at the low speed set point 110.

The comparison between the low and high penetration 12-lobed mixers, 12CL and 12UH shows that the spectrum levels of the 12UH mixer are a little lower than the 12CL mixer in low frequency ranges. However, when the frequencies are higher than 1 and 1.5 kHz at the set points 110 and 310, respectively, the noise levels of the 12UH mixer is much higher than the 12CL mixer.

The 20-lobed 20UH mixer has lower spectrum levels than the 12-lobed 12UH mixer in the high frequency range above about 1 or 1.5 kHz. The low frequency noise of the 20UH mixer was slightly increased.

Introducing a deep scallop was very successful in reducing mixer noise. The narrowband spectrum levels of the 20-lobed high penetration mixer with deep scallop, 20DS are lower than the 20UH and 12UH mixers in all frequencies at both set points 110 and 310.

Appendix A
Microphone Coordinates

TABLE A.1.—COORDINATES OF THE MICROPHONES IN THE FLOOR ARRAY

	Floor 16 mic array			L0 exit (x=0)		L1 exit (x=-2.67)		L2 exit (x=-5.43)		Mixer Plane (x=-11.06)	
mic	x	y	z	r	angle	r	angle	r	angle	r	angle
1	-20.49	-65.86	-111.19	130.84	80.99	130.45	82.15	130.11	83.35	129.57	85.83
2	-8.95	-65.79	-111.19	129.51	86.04	129.35	87.22	129.24	88.44	129.21	90.94
3	1.01	-65.74	-111.19	129.17	90.45	129.22	91.63	129.33	92.85	129.73	95.34
4	9.57	-65.68	-111.19	129.49	94.24	129.72	95.41	130.01	96.63	130.78	99.08
5	16.90	-65.64	-111.19	130.22	97.46	130.59	98.62	131.03	99.81	132.11	102.22
6	23.13	-65.60	-111.19	131.15	100.16	131.65	101.30	132.22	102.47	133.55	104.83
7	28.41	-65.57	-111.19	132.17	102.41	132.77	103.54	133.45	104.69	134.98	107.00
8	32.85	-65.55	-111.19	133.18	104.28	133.87	105.39	134.63	106.52	136.33	108.79
9	37.29	-65.52	-111.19	134.34	106.12	135.10	107.20	135.94	108.32	137.82	110.54
10	42.57	-65.49	-111.19	135.88	108.26	136.74	109.32	137.68	110.40	139.74	112.57
11	48.80	-65.45	-111.19	137.94	110.72	138.91	111.75	139.96	112.80	142.23	114.89
12	56.13	-65.41	-111.19	140.68	113.51	141.77	114.50	142.94	115.51	145.45	117.51
13	64.69	-65.36	-111.19	144.29	116.64	145.50	117.58	146.80	118.53	149.57	120.43
14	74.65	-65.30	-111.19	148.99	120.07	150.35	120.95	151.79	121.84	154.83	123.61
15	86.19	-65.23	-111.19	155.07	123.77	156.57	124.58	158.15	125.40	161.48	127.03
16	99.51	-65.15	-111.19	162.82	127.67	164.46	128.41	166.19	129.16	169.80	130.63

TABLE A.2.—COORDINATES OF THE MICROPHONES
IN THE OVERHEAD ARRAY

	Overhead 16 mic array			L0 exit (x=0)		L1 exit (x=-2.67)		L2 exit (x=-5.43)	
mic	x	y	z	r	angle	r	angle	r	angle
1	91.04	50.18	106.32	148.69	127.75	150.34	128.56	152.08	129.37
2	77.56	50.85	106.08	140.90	123.40	142.39	124.29	143.96	125.20
3	66.08	51.42	105.87	134.98	119.31	136.31	120.29	137.72	121.28
4	56.12	51.92	105.70	130.45	115.48	131.62	116.53	132.87	117.60
5	47.66	52.34	105.55	127.09	112.03	128.11	113.13	129.22	114.26
6	39.99	52.72	105.41	124.46	108.74	125.34	109.90	126.31	111.07
7	34.28	53.00	105.31	122.78	106.21	123.55	107.40	124.40	108.61
8	28.75	53.28	105.21	121.39	103.70	122.05	104.92	122.79	106.16
9	24.42	53.49	105.13	120.46	101.69	121.03	102.93	121.68	104.20
10	19.92	53.72	105.05	119.66	99.58	120.13	100.84	120.68	102.13
11	14.52	53.99	104.96	118.92	97.01	119.27	98.29	119.70	99.60
12	8.31	54.29	104.85	118.36	94.03	118.58	95.31	118.87	96.64
13	1.17	54.65	104.72	118.13	90.57	118.19	91.86	118.31	93.20
14	-7.35	55.07	104.57	118.41	86.44	118.28	87.73	118.20	89.07
15	-17.56	55.58	104.39	119.56	81.56	119.20	82.82	118.88	84.14
16	-28.92	56.14	104.19	121.83	76.27	121.23	77.50	120.66	78.78

Appendix B
Flow Conditions

The actual test conditions are given in the following tables (nprc: core pressure ratio, nprb: bypass pressure ratio, ntrc: core temperature ratio, ntrb: bypass temperature ratio, vstdc: core standard velocity, vstdb: bypass standard velocity, mfj: freejet Mach number, pabr: barometric pressure, humin: humidity inside dome, tempin: temperature inside dome, wactc: measured core flow).

TABLE B.1.—TEST CONDITIONS FOR THE FLOOR PHASED ARRAY TESTS

icrdg	setpoint	nprc	nprb	ntrc	ntrb	vstdc	vstdb	mfj	pbar	humin	tempin	wactc
1745	5000.00	1.3736	1.3707	0.9888	0.9815	730.9	725.9	0.005	14.37	37.5	537	4.751
1746	110.00	1.3911	1.4344	2.8002	1.1989	1255.9	855.6	0.006	14.36	36.4	539	2.654
1753	310.00	1.7354	1.8182	3.3377	1.1989	1748.9	1083.6	0.007	14.37	38.8	538	3.123
1775	5000.00	1.3603	1.3564	1.0028	0.9787	725.2	713.2	0.009	14.44	40.9	542	4.317
1778	310.01	1.7462	1.8197	3.3054	1.1865	1749.5	1078.7	0.015	14.43	40.7	543	2.811
1779	110.01	1.3921	1.4406	2.7947	1.1907	1256	857.5	0.014	14.43	39.1	544	2.29
1784	310.00	1.7412	1.8174	3.3344	1.1973	1753.1	1082.5	0.016	14.42	41.5	543	2.972
1785	110.01	1.3911	1.4467	2.7959	1.1933	1255	863	0.017	14.41	40.7	543	2.38
1789	310.02	1.7419	1.8276	3.2875	1.1976	1741.1	1087.3	0.018	14.41	47	541	2.984
1790	110.00	1.3884	1.4412	2.7932	1.2002	1250.8	861.3	0.018	14.42	48.5	540	2.39
1792	5000.00	1.4335	1.4343	1.07	0.9954	807.4	779.3	0.018	14.42	54.1	538	4.612
1795	310.01	1.7493	1.8313	3.3353	1.201	1759.9	1090.5	0.019	14.42	56.8	537	3.147
1796	110.00	1.3889	1.4452	2.7939	1.1944	1251.6	862.3	0.018	14.43	57.1	537	2.489
1832	1111.42	1.4378	1.4348	1.0838	0.9958	815.8	779.8	0.077	14.26	64.1	535	4.685
1835	311.05	1.7312	1.8184	3.3352	1.1976	1744.2	1082.9	0.096	14.25	67.6	534	2.88
1836	111.29	1.3936	1.4388	2.8043	1.1979	1259.7	858.4	0.071	14.25	67.4	535	2.442
1840	5000.00	1.4296	1.436	1.1579	1.0034	836.9	783.6	0.007	14.26	69.6	533	4.21
1842	310.00	1.7426	1.8209	3.3415	1.2008	1755.5	1085.5	0.009	14.26	71.1	533	2.883
1843	110.00	1.3902	1.4407	2.8092	1.1962	1256.3	859.3	0.003	14.26	71	533	2.292
1845		1.0518	1.026	3.1763	1.041	532.8	217.6	0.004	14.26	71.6	533	1.484
1846		1.0729	1.0234	3.1823	1.053	628.7	207.9	0.004	14.26	71	534	1.796
1847		1.1038	1.022	3.1796	1.059	742.9	202.1	0.004	14.26	69.5	534	2.197
1848		1.1375	1.0233	3.1813	1.0637	847.2	208.7	0.007	14.26	69.4	535	2.534
1849		1.1735	1.0232	3.1841	1.0677	942.8	208.5	0.005	14.26	70.6	534	2.897
1850		1.2214	1.0231	3.1799	1.0724	1050.8	208.3	0.004	14.26	70.8	534	3.263
1851		1.2821	1.023	3.1882	1.0751	1169.4	208.2	0.005	14.26	71.7	534	3.77
1852		1.3433	1.0229	3.1747	1.0809	1268.1	208.5	0.004	14.26	73.8	533	4.18
1853		1.4212	1.0228	3.1962	1.0826	1383.8	208.3	0.002	14.26	74.6	532	4.576

TABLE B.2—TEST CONDITIONS FOR THE OVERHEAD PHASED ARRAY TESTS

icrdg	setpoint	nprc	nprb	ntrc	ntrb	vstdc	vstdb	mfj	pbar	humin	tempin	wactc
1564	310.03	1.7507	1.8364	3.2399	1.1946	1735	1089.6	0.008	14.23	41.7	551	2.795
1566	110.02	1.3958	1.4169	2.7902	1.2035	1259.5	843	0.010	14.23	44.2	549	2.488
1583	110.01	1.3944	1.4436	2.8141	1.2029	1263.3	864.2	0.011	14.33	33	538	2.506
1584	310.01	1.7446	1.8253	3.358	1.203	1762	1088.7	0.010	14.33	35	536	3.035
1589	110.01	1.3945	1.4421	2.8151	1.2005	1263.7	862.2	0.012	14.32	34.8	537	2.57
1590	310.00	1.7345	1.8167	3.3402	1.1974	1748.8	1082.3	0.012	14.32	34	538	3.08
1594	110.01	1.3843	1.4407	2.8075	1.1957	1248.5	859.3	0.014	14.31	35.6	538	2.576
1596	310.01	1.7384	1.8244	3.3471	1.2004	1753.9	1087.1	0.014	14.31	35.4	538	3.188
1600	110.01	1.3907	1.4424	2.8263	1.2044	1261.3	863.8	0.016	14.31	41.3	535	2.552
1603	310.02	1.7505	1.831	3.389	1.2066	1775.1	1092.9	0.015	14.31	42.8	534	3.145
1607	310.02	1.7382	1.8206	3.3781	1.2189	1761.7	1093.7	0.014	14.33	54	530	3.025
1608	110.02	1.3945	1.4411	2.8481	1.2149	1271.1	866.5	0.012	14.33	54.5	529	2.512
1617	5000.07	1.3719	1.3698	0.9819	0.9831	727	725.7	0.007	14.42	41.6	538	4.559
1621	110.00	1.3895	1.4396	2.7917	1.1952	1251.9	858.3	0.010	14.41	41.4	537	2.465
1622	310.00	1.737	1.8177	3.3261	1.1962	1747.1	1082.2	0.010	14.41	44.5	537	3.03
1623	5000.06	1.3805	1.3814	1.0924	0.9977	774.1	740.3	0.010	14.40	56.7	536	4.54
1626	310.00	1.7374	1.8158	3.3276	1.1985	1747.8	1082.3	0.012	14.40	56.3	536	3.071
1627	110.01	1.3925	1.4395	2.7867	1.1943	1254.6	857.9	0.013	14.40	54.1	536	2.534
1629	5000.02	1.4217	1.4231	1.1273	1.0088	819.8	776.4	0.012	14.40	47.3	536	4.468
1632	310.01	1.7442	1.8248	3.3319	1.2	1754.7	1087.1	0.010	14.40	51.9	535	3.022
1633	110.01	1.3891	1.438	2.812	1.2019	1255.9	859.4	0.011	14.40	52.8	534	2.446
1635	5000.02	1.4214	1.4198	1.1808	1.0159	838.8	776.7	0.011	14.41	61.8	530	4.458
1638	310.02	1.746	1.8253	3.3751	1.2127	1767.6	1093	0.013	14.41	59.7	531	3.058
1639	110.02	1.3899	1.441	2.8276	1.2098	1260.4	864.6	0.012	14.41	58.9	531	2.472
1650	5000.07	1.3713	1.372	1.0185	0.9965	740	732.6	0.007	14.35	51.4	540	4.426
1652	310.01	1.7481	1.8243	3.3344	1.1999	1758.7	1086.8	0.011	14.34	48.4	540	3.021
1653	110.00	1.3954	1.4413	2.8007	1.195	1261.7	859.5	0.009	14.34	46.4	540	2.494
1656	5000.05	1.3862	1.3848	1.1107	1.0046	785.2	745.7	0.004	14.33	44.7	538	4.497
1659	310.01	1.7471	1.8228	3.3616	1.207	1765	1089.4	0.006	14.33	47.7	537	3.074
1660	110.01	1.3931	1.4403	2.8035	1.2011	1259.2	860.9	0.003	14.33	47.6	537	2.54
1663	5000.04	1.3983	1.3946	1.1558	1.005	811.1	753.5	0.008	14.33	48.7	535	4.565
1665	310.01	1.744	1.8229	3.3224	1.1958	1751.9	1084.4	0.006	14.33	49.3	535	3.186
1666	110.00	1.3865	1.4372	2.7931	1.1972	1248.2	857.2	0.004	14.33	50	535	2.56
1670	5000.07	1.374	1.3729	1.0991	0.9951	771	732.6	0.007	14.33	55.2	534	4.631
1672	310.00	1.738	1.824	3.3251	1.1972	1747.6	1085.5	0.006	14.33	54.7	534	3.255
1673	110.00	1.3911	1.4434	2.7914	1.1955	1253.9	861.3	0.006	14.33	54.7	534	2.703
1683	2004.06	1.3558	1.3537	1.013	0.9868	725.2	713.9	0.007	14.29	59.5	541	4.32
1685	310.03	1.7459	1.8239	3.234	1.1985	1729.9	1086	0.008	14.28	62	540	2.938
1686	110.01	1.4001	1.4441	2.804	1.198	1268.5	862.8	0.008	14.28	61	541	2.439
1690	310.01	1.7384	1.8178	3.3153	1.1924	1745.6	1080.5	0.006	14.26	60.7	540	2.69
1691	110.00	1.3868	1.4401	2.7942	1.1949	1248.9	858.5	0.006	14.26	58.9	541	2.212
1695	310.01	1.7445	1.8259	3.3255	1.1974	1753.3	1086.4	0.006	14.25	59	540	2.748
1696	110.00	1.3905	1.4409	2.7904	1.1945	1252.9	859	0.005	14.25	57.1	540	2.221
1700	310.00	1.7429	1.8252	3.3294	1.1987	1753	1086.7	0.008	14.25	58.9	539	2.772
1701	110.00	1.3842	1.4388	2.794	1.1962	1245.3	858	0.009	14.25	58.7	539	2.225
1705	310.00	1.7361	1.8189	3.3256	1.1947	1746.2	1082	0.008	14.26	60.9	538	3.117

TABLE B.2—CONCLUDED.

1706	110.00	1.3879	1.4394	2.792	1.1953	1249.8	858.1	0.007	14.26	64	537	2.526
1713	5000.05	1.3865	1.3834	0.9874	0.9859	740.6	737.6	0.005	14.23	73.8	531	1.288
1720	5000.06	1.3768	1.3747	0.9826	0.981	731.2	728.8	0.007	14.29	63	532	4.567
1725	310.00	1.7426	1.817	3.3385	1.1946	1755.1	1081.1	0.007	14.29	59.7	532	3.039
1726	110.01	1.3889	1.4446	2.787	1.196	1249.9	862.4	0.004	14.29	60.1	532	2.34
1729	5000.04	1.4047	1.4022	1.0844	0.9953	790.7	755.6	0.006	14.29	65.9	531	4.603
1731	310.00	1.741	1.8222	3.3313	1.1936	1751.7	1083	0.003	14.29	68	531	3.078
1732	110.01	1.3831	1.4419	2.8056	1.1955	1246.5	860.2	0.004	14.29	67.8	531	2.312
1735	2004.07	1.366	1.3652	1.1255	1.0025	773.3	729.1	0.003	14.30	66.5	529	4.378
1737	310.01	1.7498	1.8271	3.3404	1.1962	1761.6	1086.4	0.005	14.31	67.4	529	3.236
1738	110.00	1.3921	1.4454	2.7933	1.197	1255.6	863.4	0.004	14.31	66.3	530	2.506

References

1. Mengle, V.G., Baker, V.D., and Dalton, W.N., Lobed mixer Design for Noise Suppression, NASA/CR—2002-210823, 2002.
2. Tester, B.J. and Fisher, M.J., Understanding and prediction of jet noise generation by forced mixers, AIAA–2004–2897.
3. Bridges, J. and Wernet, M.P., Cross-stream PIV measurements of jets with Internal Lobed Mixers, AIAA–2004–2896.
4. Dougherty, R.P., Beamforming in acoustic testing, in Aeroacoustic Measurements, Mueller, T.J. (ed.), 2002.
5. Underbrink, J.R., Aeroacoustic phased array testing in low speed wind tunnel, in Aeroacoustic Measurements, Mueller, T.J. (ed.), 2002.
6. Johnson, P. and Dudgeon, D., Array signal processing: Concepts and techniques, Prentice Hall, New Jersey, 1993.

REPORT DOCUMENTATION PAGE

Form Approved
OMB No. 0704-0188

Public reporting burden for this collection of information is estimated to average 1 hour per response, including the time for reviewing instructions, searching existing data sources, gathering and maintaining the data needed, and completing and reviewing the collection of information. Send comments regarding this burden estimate or any other aspect of this collection of information, including suggestions for reducing this burden, to Washington Headquarters Services, Directorate for Information Operations and Reports, 1215 Jefferson Davis Highway, Suite 1204, Arlington, VA 22202-4302, and to the Office of Management and Budget, Paperwork Reduction Project (0704-0188), Washington, DC 20503.

1. AGENCY USE ONLY (*Leave blank*)	2. REPORT DATE	3. REPORT TYPE AND DATES COVERED
	September 2005	Final Contractor Report

4. TITLE AND SUBTITLE

Phased-Array Study of Jets With Various Internal Mixers and Nozzles

5. FUNDING NUMBERS

WBS–22–781–30–63
SAA3–456

6. AUTHOR(S)

Sang Soo Lee

7. PERFORMING ORGANIZATION NAME(S) AND ADDRESS(ES)

QSS Group, Inc.
21000 Brookpark Road
Cleveland, Ohio 44135

8. PERFORMING ORGANIZATION REPORT NUMBER

E–15240

9. SPONSORING/MONITORING AGENCY NAME(S) AND ADDRESS(ES)

National Aeronautics and Space Administration
Washington, DC 20546–0001

10. SPONSORING/MONITORING AGENCY REPORT NUMBER

NASA CR—2005-213870

11. SUPPLEMENTARY NOTES

Project Manager, Edmane Envia, Propulsion Systems Division, NASA Glenn Research Center, organization code RTA, 216–433–8956.

12a. DISTRIBUTION/AVAILABILITY STATEMENT

Unclassified - Unlimited
Subject Categories: 07 and 34

Available electronically at http://gltrs.grc.nasa.gov

This publication is available from the NASA Center for AeroSpace Information, 301–621–0390.

12b. DISTRIBUTION CODE

13. ABSTRACT ***(Maximum 200 words)***

The 16 microphone linear phased-array system has been successfully applied to identify the noise source locations. The various mixers and nozzles increase or decrease noise levels of certain frequency components. The phased-array beamforming can show the locations of these added/decreased noise sources. It was also able to detect any internal rig noise that is shown to be coming from the nozzle exit. Major beamforming level differences between nozzles occurs at the nozzle exit. Among the three nozzles tested, the medium length nozzle was the quietest for all mixers. The spectrum levels of the high penetration 12-lobed mixer are much higher than the low penetration mixer in the frequency ranges higher than 1 or 1.5 kHz. The high penetration 20-lobed 20UH mixer has lower spectrum levels than the 12-lobed mixer in the high frequency range above about 1 or 1.5 kHz. Introducing a deep scallop was successful in reducing mixer noise in most frequencies.

14. SUBJECT TERMS

Jets; Noise reduction; Aeroacoustics; Turbofan engines; Acoustics; Propulsion; Flight; Exhaust nozzles; Mixers; Beamforming; Far field; Microphones; Noise intensity; Free jets

15. NUMBER OF PAGES

46

16. PRICE CODE

17. SECURITY CLASSIFICATION OF REPORT	18. SECURITY CLASSIFICATION OF THIS PAGE	19. SECURITY CLASSIFICATION OF ABSTRACT	20. LIMITATION OF ABSTRACT
Unclassified	Unclassified	Unclassified	